1 **High precision osmium stable isotope measurements by double spike MC-ICP-MS and N-TIMS.**
2

3 Josefine A.M. Nanne*[a], Marc-Alban Millet [a,b], Kevin W. Burton[a], Chris W. Dale[a], Geoff M. Nowell[a] and Helen
4 M. Williams [a,c]
5

6 * Corresponding author. E-mail: j.a.nanne@durham.ac.uk

7   a. Department of Earth Sciences,
8   Durham University,
9   Science Labs, South Road,
10   Durham DH1 3LE, United Kingdom.
11

12   b. *Present address:* School of Earth and Ocean Sciences,
13   Cardiff University,
14   Main building, Park Place,
15   Cardiff CF10 3AT, United Kingdom.
16

17   c. *Present address:* Department of Earth Sciences,
18   The University of Cambridge,
19   Downing Street,
20   Cambridge CB2 3EQ, United Kingdom.
21

22 **ABSTRACT**

23 Osmium stable isotopes provide a new, potentially powerful tool with which to investigate a diverse

24 range of geological processes including planetary formation, ore-genesis and weathering. In this paper,

25 we present a new technique for high precision measurement of osmium (Os) stable isotope ratios by

26 both Multiple-Collector Inductively Coupled Plasma Mass Spectrometry (MC-ICP-MS) and Negative ion

27 Thermal Ionisation Mass Spectrometry (N-TIMS). We use a 188Os-190Os double spike, composed of

28 61% 188Os and 39% 190Os, to correct for mass dependent fractionation resulting from sample

29 preparation and isotope measurement, with the ideal spike to sample ratio being 55:45. Isotope ratios

30 are expressed as δ190Os which is the per mil deviation in the measured 190Os/188Os ratio relative to

31 isotope reference material DROsS. Repeated analyses of double spiked DROsS for both MC-ICP-MS (n=

32 80 cycles) and N-TIMS (n= 280 cycles) show that an internal precision of 0.01-0.02 ‰ on δ190Os (2 se)

33 can be attained, with a long-term reproducibility of 0.016 ‰ and 0.029 ‰ (2 sd; n = 91 and 83,

34 respectively). The better reproducibility on MC-ICP-MS than on N-TIMS is, predominantly, due to

35 measurement at higher beam intensities (11-18 V with consumption of ~200 ng natural Os vs. 2-18 V

36 with consumption of 2.3 – 45 ng natural Os, respectively). In addition to stable isotope compositions,

37 our method allows for simultaneous measurement of 187Os/188Os and 186Os/188Os ratios with a

38 precision of <40 ppm (2 se; 80 cycles for MC-ICP-MS and 280 cycles for N-TIMS) and an external

39 reproducibility of 123-268 ppm and 234-361 ppm (2 sd; n= 91 for MC-ICP-MS and n= 83 for N-TIMS),

40 respectively. We demonstrate that a similar precision and reproducibility can be obtained for other

41 pure Os solutions as well as for geological materials. In addition, a range of analytical tests evaluates

42 and demonstrates the robustness of our method with regards to residual matrix effects and

43 interference correction, signal intensity and on-peak zero on MC-ICP-MS, and the effect of oxygen

44 corrections and isobaric interference on N-TIMS. Finally, we report the first Os stable isotope

45 compositions for geological reference materials, including mantle peridotites and chromitites, and one

46 ordinary chondrite.

47

1. INTRODUCTION

Osmium (Os) has two radiogenic isotopes ([186]Os and [187]Os) and five naturally occurring stable isotopes: [184]Os, [188]Os, [189]Os, [190]Os, and [192]Os, with relative abundances of 0.02 %, 13.21 %, 16.11 %, 26.21 %, and 40.74 %, respectively. Osmium is a refractory and highly siderophile (Fe-loving) element and is therefore of considerable interest in the study of planetary differentiation and formation of Earth's metallic core. It is also a chalcophile (S-loving) element, and strongly partitions into sulphides. Consequently, Os behaves compatibly during mantle melting, where sulphide remains as a residual phase in the source. Taking advantage of the chemical properties of Os and the differences in behaviour between Re, Pt and Os, the [187]Re-[187]Os and [190]Pt-[186]Os decay systems have become important chronometers and tracers in both high and low-temperature geochemistry [e.g.1, 2]. More specifically, these radiogenic isotope systems have been used to study early solar system dynamics [e.g. 3, 4], planetary differentiation processes [e.g. 5, 6], mantle heterogeneity [e.g. 7, 8], crustal growth and recycling [e.g. 9-11], economic mineralization in ore deposits [e.g. 12], and the nature of weathering processes associated with brief climatic excursions [e.g. 13-15]. However, despite the potential to use stable Os isotopes to investigate these same processes, thus far this system remains unexplored.

A potential limitation for the use of Os stable isotopes in geochemistry is the small range of natural variation expected for high-mass elements. This is compounded by the very low abundance of Os in most terrestrial samples. However, recent advances in mass spectrometry and development of new techniques for stable isotope measurement have led to the discovery of significant and systematic stable isotope fractionation for high-mass stable isotope systems in both high and low-temperature environments[16-22]. This suggests that Os stable isotope variations may be measurable if a suitable high precision analytical method can be developed.

Additional complications that must be addressed in order to successfully measure Os stable isotopes include the non-quantitative recovery of Os during sample processing (typically on 60-80 %[23, 24]) and instrumental mass bias (MC-ICP-MS) or mass fractionation (N-TIMS) during measurement. Such fractionation can be overcome by the use of a double spike (DS) [25]. This approach has been shown to reliably account for mass-dependent stable isotope fractionation that can occur during all steps of sample processing (digestion, chemical separation and mass spectrometry) [18, 26, 27].

In this paper, we present a new method for the measurement of high-precision stable Os isotope ratios using a [188]Os-[190]Os double spike by both plasma source (MC-ICP-MS) and negative thermal ionisation mass spectrometry (N-TIMS). Method development on both machines allows for the analysis of sample materials over a broad range of Os concentrations (>1 ppb) at precisions of 0.01-0.02 ‰ on δ^{190}Os (2 se; 80 cycles for MC-ICP-MS and 280 cycles for N-TIMS). In addition, we show that the method allows for simultaneous collection of stable isotopes and radiogenic isotope ratios, [187]Os/[188]Os and [186]Os/[188]Os, at a precision of <40 ppm (2 se; 80 cycles for MC-ICP-MS and 280 cycles for N-TIMS). We show the robustness, precision and accuracy of our method through a range of analytical tests and

84 repeated measurements of pure Os solutions and geological materials. Finally, data is presented for a

85 range of geological materials.

86

87 **2. OSMIUM DOUBLE SPIKE METHODOLOGY**

88 **2.1 Osmium Double Spike Design**

89 The double spike (DS) approach requires four stable isotopes that are related to each other by mass-

90 dependent stable isotope fractionation. For Os we can use ^{188}Os, ^{189}Os, ^{190}Os, and ^{192}Os. Departures

91 from mass-dependent fractionation, either due to cosmogenic effects or nucleosynthetic anomalies,

92 have not been detected in terrestrial samples but have been reported for extra-terrestrial materials.

93 Components of carbonaceous chondrites display mass independent Os isotopic anomalies although

94 homogeneity is shown at the bulk meteoritic scale [e.g. 28, 29,30]. Mass independent anomalies at the bulk

95 rock scale have been shown for iron meteorites [e.g. 31] which should be considered when analysing such

96 meteorites.

97   The DS deconvolution used in this study is based on the geometric iterative resolution method

98 of Siebert et al. (2001)[32]. Measurements were also double checked using an algebraic resolution

99 method used by Millet and Dauphas (2014)[33] and Millet et al. (2016)[34] which yielded identical results.

100 Regardless of the approach, the DS deconvolution consists of resolving the following non-linear

101 equation:

$$R_m = \left[(1-f)R_{standard}(i_x/i_n)^\alpha + fR_{spike}\right] * (i_x/i_n)^\beta$$

103 where R_m, $R_{standard}$ and R_{spike} are the measured, standard and spike isotope ratios; i_n is the atomic weight

104 of the normalising isotope (^{188}Os); i_x is the atomic weight of one of the three other isotopes used to

105 resolve the equation which in our method are ^{189}Os, ^{190}Os and ^{192}Os; f is the relative proportion of ^{188}Os

106 originating from the spike in the sample–spike mixture; α is the natural and β the processing and

107 instrumental exponential fractionation factors. In this study, reference material DROsS has been used

108 as standard. All Os stable isotope compositions are thus reported relative to DROsS, as the per mil

109 deviation (‰) of the $^{190}Os/^{188}Os$ ratios, here after reported as $\delta^{190}Os$:

$$\delta^{190/188}Os_{DROsS} = \left(\frac{\frac{190}{188}Os_{sample}}{\frac{190}{188}Os_{DROsS}} - 1\right) * 1000$$

111 Radiogenic isotopes ^{186}Os and ^{187}Os are not used in the DS deconvolution. Consequently, the spike

112 proportion, and the geological and analytical fractionation factors resolved within the DS deconvolution

113 can be used to calculate the $^{186}Os/^{188}Os$ and $^{187}Os/^{188}Os$ ratios. Osmium concentrations were

114 determined by performing isotope dilution calculations.

115   The analytical uncertainty on double spike measurements is highly dependent on spike

116 composition and sample-spike mixing proportions. To establish the optimal composition and

117 proportions for Os, we have modelled the internal precision of a typical MC-ICP-MS measurement

118 following the model of Millet and Dauphas (2014)[33] which takes into account the errors associated to

119 Johnson noise and counting statistics (see ref. 33 for more details). This error model differs from that

120 of Rudge et al. (2009)[35] in that i) errors on the natural fractionation factor (alpha) are calculated on the

121 basis of a constant intensity for the most abundant isotope in the natural Os-DS mixture, rather than

122 calculated based on a constant total Os ion beam and; ii) determination of errors is done through Monte

123 Carlo modelling. In our model, the maximum intensity for the most abundant isotope was set at 6 V. A

124 measurement is assumed to comprise 80 cycles with an integration time of 8.3 seconds per cycle on

125 $10^{11}\,\Omega$ collectors at T=290 K. The model shows that a minimum internal error, of ~0.010 ‰ amu^{-1} (2 se),

126 is acquired when using a 0.6:0.4 ^{188}Os – ^{190}Os mixed spike composition and a 0.55:0.45 spike-sample

127 mixture (Fig. 1). This is close to the optimal double spike composition as calculated by Rudge et al.

128 (2009)[35] of 0.66:0.34 ^{188}Os -^{190}Os for a 0.6:0.4 spike-sample mixture. It is important to note that the 2

129 se error is <0.020 ‰ amu^{-1} when the sample proportion ranges between 15 % and 81 %. That errors

130 are minimal over a large range of spike-sample mixtures is of great utility when the Os concentration

131 of samples is not well known. A triple spike composition was considered in our calculations but was not

132 found to improve precision.

133

134 **2.2 Preparation and calibration of ^{188}Os – ^{190}Os double spike**

135 Single ^{188}Os and ^{190}Os isotope spikes were purchased as fine-grained metallic powders from Trace

136 Sciences International. In order to ensure purity of the double spike, the metal powders were

137 individually digested using Carius tubes, followed by extraction and purification as described in section

138 3.2. Individual spikes were subsequently mixed in calculated optimal proportions and the resulting

139 double spike was diluted with 3 M HCl to desired concentrations.

140   Calibration of the double spike isotope composition was achieved by measuring a pure

141 standard and pure double spike solution as well as a range of Durham Romil Osmium Standard (DROsS[36,

142 [37])-DS mixtures. Practically, this involves iterative correction for instrumental mass fractionation of the

143 pure DS measurements to generate a putative true DS composition, with an initial estimate provided

144 by the pure DROsS analysis. This putative true DS composition is then fed into the DS deconvolution

145 and used on all DS-DROsS mixtures, ranging from 0.1:0:9 to 09:0.1 mixing proportions. Calibration is

146 considered satisfactory once most mixtures, especially those around the optimum mixture proportions,

147 display a δ^{190}Os within analytical error of zero. For all these solutions, Carius tubes were used to ensure

148 standard-sample equilibration. Measurements were carried out by MC-ICP-MS with each analysis

149 comprising 220 cycles of 8.39 seconds and were all preceded by on-mass on-peak zero measurement

150 (20 integrations of 8.39 seconds). The isotope composition of the DS and of reference standard DROsS,

151 as used in the calibration and stable isotope calculations, can be found in Table 1.

152

153   **3. MATERIALS AND SAMPLE PROCESSING**

154   **3.1 Materials and samples**

155   Digestion and processing of standards and samples were carried out at Durham University. During the
156   course of this study, we used Romil acids of variable grades (Super Purity Acids and Ultra Purity Acids)
157   with blank levels suitable for the analytical procedure. The nitric acid was purified by sparging with
158   filtered air. Acid dilutions were performed with ultrapure (18.2 MΩ·cm) water.

159   We use the Durham Romil Osmium Standard (DROsS)[36, 37] as a reference standard. This is an
160   international Os isotope reference material supplied by IAGeo Limited that has been widely distributed
161   [e.g.38, 39] and for which Os isotope ratios have been determined to high precision and accuracy by both
162   MC-ICP-MS[36] and N-TIMS[37]. For method testing, we have also measured three in-house pure Os
163   reference solutions, ROMIL, SpecPure, and OsCaR, which were purchased from Romil Ltd, Alfa Aesar,
164   and provided by A. Poirier (OsCaR). As representative rock samples, we used well-characterized and
165   commonly used reference materials: peridotites UB-N[40] and GP-13[41], and chromitites CHR-Bkg[42, 43] and
166   CHR-Pt+[44]. Reference material GP-13 is an in-house PGE standard prepared at Durham University which
167   has been widely distributed. The other materials, UB-N, CHR-Bkg and CHR-Pt+, are distributed by CRPG-
168   CRNS, Nancy, France. Furthermore, we included an ordinary H-chondrite, ZAG. These samples were
169   chosen to reflect the range of Os concentrations and sample matrices available for study.

170

171   **3.2 Sample digestion and chemical purification of Os**

172   Samples were digested either by Carius tube (CT)[23, 45] or high-pressure asher (HPA, Anton Paar)[44], with
173   respective maximum of 2.5 g and 2 g powder material per tube. Digestions were performed using
174   inverse aqua regia (1:2; 12 M HCl: 16 M HNO$_3$) for ≥16 h at temperatures of 230°C in the case of CT and
175   290-310°C for HPA digestions. The double spike was added to each tube prior to sample digestion. After
176   digestion, the extraction and purification of Os closely followed techniques described by Cohen et al.
177   (1996)[21] and Birck et al. (1997)[22]. Separation of Os from the aqua regia digest solution was achieved by
178   solvent extraction using CHCl$_3$[46]. Osmium was then back-extracted from the chloroform solution using
179   concentrated HBr and subsequently purified using the micro-distillation procedure of Roy-Barman
180   (1993)[47] as described by Birck et al. (1997)[24]. In the case of measurements by MC-ICP-MS, samples were
181   evaporated and chlorified three times using 300 µL of 8 M HCl before being taken up in 3 M HCl to a
182   total Os concentration of ~0.5 µg mL^{-1}. When performing Os analyses by N-TIMS, samples were dried
183   down after microdistillation to approximately 1-2 µL of sample solution and then loaded onto a Pt
184   ribbon filament. Typical total procedural blanks range between 0.01 and 0.10 pg Os which is similar to
185   previous Os studies carried out at Durham University [e.g. 48].

186

187   **4. MASS SPECTROMETRY**

188 Osmium isotope ratios were measured at Durham University on a ThermoFisher Scientific Neptune MC-

189 ICP-MS[36] and a Triton Plus N-TIMS[37, 39, 49]. The use of both MC-ICP-MS and N-TIMS allowed us to exploit

190 the advantages of the different ionisation sources and provide a means to assess the relative accuracy

191 of each measurement. The overall introduction and ionisation efficiency of MC-ICP-MS is relatively low

192 (~0.08 %[36]) which makes it better suited for analysing large samples and calibrating standards. The

193 advantage of the MC-ICP-MS is that Os is measured as Os^+ which makes the mass spectrum relatively

194 simple and corrections for isobaric interferences relatively straightforward. By contrast, N-TIMS has a

195 much higher ionisation efficiency for Os (1-5 %[37]) which makes it ideal for samples with a low Os

196 abundance or when sample material is limited. However, Os is measured as the tri-oxide ion OsO_3^-

197 which makes the mass spectrum complex and necessitates multiple oxide corrections that add to the

198 overall uncertainty. In both cases, internal errors are presented as the 2 se on $\delta^{190}Os$ of each integration,

199 once passed through a 2 se filter to remove outliers.

200

201 **4.1 MC-ICP-MS**

202 *4.1.1 Instrument set-up and parameters MC-ICP-MS*

203 The Neptune MC-ICP-MS was set-up for static simultaneous collection of all Os isotopes, apart from the

204 least abundant ^{184}Os. We also collected ^{183}W, ^{185}Re, and ^{194}Pt in order to monitor and correct for isobaric

205 interference (Table 2). In this study, interference beam intensities were <0.05 mV for ^{183}W, <0.01 mV

206 for ^{185}Re, and <0.5 mV for ^{194}Pt. Typical instrument operating conditions were similar to those outlined

207 in Nowell et al. (2008)[36]. Sample material was introduced in 3 M HCl using an Elemental Scientific

208 Incorporated (ESI) PFA-50 micro-flow nebuliser and Glass Expansion (GE) micro-cyclonic "Cinnabar"

209 spray-chamber. During typical run conditions, the measured sample uptake rate was ca. 80 µL min^{-1}

210 with a sensitivity of ca. 30 V ppm^{-1}. Measurements were carried out in static mode in 1 block of 80

211 cycles of 8.389 seconds integration time each. Mass calibration was updated by peak-centering on the

212 centre-cup mass ^{188}Os at the start of each session and checked again at the end. Prior to every sample

213 run, baselines were obtained by on-mass on-peak zero (OPZ) measurements for 20 x 8.389 seconds

214 integrations in clean 3 M HCl. Washouts between sample runs used 3 M HCl acid for at least 5 minutes

215 which resulted in the ^{188}Os beam decreasing below 2 mV (~0.03 % of the typical sample signal). Total

216 analysis time, including OPZ and wash-out, was approximately 15 minutes with consumption of 800 µL

217 sample solution (equivalent to 400 ng total Os in the case of a 0.5 µg mL^{-1} solution).

218

219 *4.1.2 Data reduction MC-ICP-MS*

220 Following analysis, all raw intensity data were exported and re-processed offline on a cycle-by-cycle

221 basis using an in-house Excel spreadsheet. For MC-ICP-MS analyses, corrections were applied in the

222 following order; baseline subtraction using the OPZ measurements, abundance sensitivity (1 ppm[36]),

223   isobaric interferences, and DS deconvolution. The abundance sensitivity is assumed to be similar to that

224   determined by Nowell et al. (2008)[36].

225

226   *4.1.2.1 Effect of beam intensity and on-peak zero*

227   To evaluate the effect of beam size on the accuracy, the main 500 ppb DROsS-DS solution was diluted

228   to various lower concentrations (100 - 5 ppb total Os; Table 3). This resulted in total Os beam intensities

229   varying between 18 V and 0.1 V, with the corresponding ^{188}Os ranging between 6.7 V and 0.005 V. All

230   analyses show Os stable isotope ratios as well as ^{187}Os/^{188}Os within analytical uncertainty of one

231   another (Fig. 2; Table 3). The ^{186}Os/^{188}Os only shows a significant deviation from the reference value

232   when the total Os beam intensity is 0.14 V, corresponding to solutions with concentrations of ~ 5 ppb

233   total Os which equals the consumption of ~4 ng total Os (i.e. natural plus DS) under standard running

234   conditions.

235   Analyses by MC-ICP-MS at low beam intensities critically rely on the absence of memory

236   effects. The on-peak zero (OPZ), used to account for baseline, can introduce an inaccuracy on the stable

237   isotope composition especially when measuring samples with very distinct isotope composition. The

238   importance of the wash-out and sample to sample memory has been discussed in detail by Nowell et

239   al. (2008)[36]. They show that when certain precautions are taken (e.g., avoid drying out of the spray

240   chamber between sessions, keep standards and samples in the same chemical form), the effect on the

241   Os isotopic composition is negligible and should not prevent the acquisition of high precision data.

242   Considering that the natural variation in stable isotope compositions is expected to be small and the

243   proportion of sample to spike are well matched, the potential of memory effect on the stable isotope

244   ratios can, therefore, assumed to be minimal. In this study, the OPZ of the diluted DROsS solutions

245   display signal intensities between 0.04 % and 0.6 % relative to the peak Os signal (^{188}Os) in the main

246   run. The accuracy of the δ^{190}Os values even at low beam intensities suggests that the OPZ has an

247   insignificant effect on the accuracy at levels up to 0.6 %. For DROsS analyses run at total Os beam

248   intensities of >10 V, OPZ analyses are in general <2 mV and <0.04 % of the peak Os signal. The potential

249   of inaccurate δ^{190}Os values as a result of OPZ analyses can, therefore, be neglected. The fact that OPZ

250   correction is less accurate for ^{186}Os/^{188}Os is partly due to the lower intensities of ^{186}Os relative to all

251   other isotopes involved in the double-spike deconvolution (^{188}Os, ^{189}Os, ^{190}Os and ^{192}Os). The ^{186}Os

252   signal of the OPZ analyses at 0.14 V is 4 % of the main run beam. On-peak zero determination is,

253   therefore, critical for obtaining reliable ^{186}Os/^{188}Os simultaneously with δ^{190}Os by MC-ICP-MS.

254   It should be noted that the higher ionisation efficiency of the N-TIMS allows for small quantities

255   of Os to be measured at higher intensities. For example, while consumption of 4 ng total Os (5 ppb

256   solution) provides a total Os beam intensities of 0.1 V by MC-ICP-MS, we typically obtain a total Os

257   beam intensity of >1 V for a total Os load of ≥5 ng by N-TIMS. Furthermore, Figure 7 shows that the

258   error is significantly increased when the ^{188}Os beam intensity drops below ~1 V (~2.7 V ^{total}Os) which is

259 an important consideration to make when small variations in stable isotope composition are expected.

260 We, therefore, recommend that measurements on less than ~100 ng of total Os be performed by N-

261 TIMS.

262

263 *4.1.2.2 Matrix effects and interference corrections*

264 Potential atomic isobaric inferences on Os isotopes can arise from the incomplete separation of Os from

265 W, Re and Pt. In addition, non-spectral matrix effects can create inaccurate results[50]. To assess if our

266 method can accurately correct for these interferences, we doped double spiked DROsS with a range of

267 elements that are (i) typically found in silicate rocks (Si, Al, Mg, Fe, Ca, Ti, Ni and Cr), (ii) dominant in

268 iron meteorites (Fe, Ni), (iii) platinum group elements (Ru, Rh, Pd, Ir, and Pt), and (iv) trace elements

269 that have direct isobaric interferences on Os (Pt, W and Re). Test solutions were doped at levels ranging

270 from 0.01-10 % of the total Os concentration. Each element was present in x% of the Os abundance,

271 e.g. Si was present at 5% of the Os abundance. All measurements display values that are within

272 analytical uncertainty of undoped DROsS measurements (Fig. 3; Table 3). This illustrates that matrix

273 effects as well as isobaric interferences, even at extreme levels of up to 10 %, can be accurately

274 accounted for. The interference beam intensities monitored for standard solutions as well as geological

275 sample material processed and analysed in this study are all <0.01 % of the total Os concentration and

276 are, therefore, not expected to introduce data inaccuracies.

277

278 **4.2 N-TIMS**

279 ***4.2.1 Instrument set-up and parameters***

280 For N-TIMS analyses, sample material was loaded onto Pt single filaments in concentrated HBr or in 3

281 M HCl when the sample solution was also measured by MC-ICP-MS. After the sample material was dried

282 down on the filament, ~0.5 µL of NaOH-Ba(OH)$_2$ activator was added to enhance ionisation. The amount

283 of Os loaded for this study varied between 2.3 and 45 ng natural Os. Where MC-ICP-MS provides fairly

284 consistent beam intensities for a certain set-up, the intensity that is obtained for a given amount of Os

285 is not directly correlated on N-TIMS, but also depends on the activator and sample loading on the

286 filament. A two-sequence static multi-collection routine was used in order to analyse masses 232 to

287 242 (Table 2). Masses 241 and 242 are collected to calculate the oxygen isotope compositions (see

288 section 4.2.2). A single analysis consists of 28 blocks, each comprising 10 cycles with 8.389 seconds

289 integration per cycle followed by 3 seconds idle time. Amplifier gain calibrations were performed at the

290 start of each day, although amplifiers were rotated throughout an analysis to cancel out amplifier gains.

291 Baseline measurements and peak centering, using masses 236 and 240, were carried out prior to every

292 run. The presence of interfering PtO$_2^-$, ReO$_3^-$, and WO$_3^-$ were quantified by measuring masses 228, 230-

293 233 by ion counter before and after each Faraday measurement for 4-6 cycles with a total analysis time

294 of 110-160 seconds. During analysis, high purity oxygen (99.6 % purity, supplied by BOC) was bled into

295 the source chamber with the pressure kept constant at ~2.5 x 10^{-7} mbar.

296

4.2.2 Data reduction N-TIMS

298 Osmium analyses by N-TIMS are performed using the tri-oxide ion (OsO$_3^-$) and, therefore, corrections

299 for the effects of variable isobaric oxygen isotope interferences of the heavier oxygen isotopes (^{17}O and

300 ^{18}O) are required. For example, correction for ^{188}Os^{16}O$_2^{17}$O$^-$ on ^{189}Os^{16}O$_3^-$ at mass 239. In this study, we

301 adopted the method of Luguet et al. (2008)[37] where the O isotope composition is determined in-run for

302 each integration so that any variation throughout an analysis can be accounted for. This is a more

303 accurate approach than using a fixed O isotope composition because the composition has been shown

304 to vary from sample to sample as well as throughout an individual run [e.g. 37, 39, 51, 52]. For comparison, we

305 have also applied the method recommended by Chatterjee and Lassiter (2015)[39] where the O isotopic

306 composition was measured before and after the main run using a separate routine. This routine

307 consisted of the second line as mentioned in Table 2 and data was collected for 10 cycles of 8.389

308 seconds integrations each. From the 20 cycles, the mean 241/238 and 242/238 values (2 se outlier

309 rejected) were taken as an approximation of the O isotopic composition of the specific run. The

310 collection of masses 241 and 242, which are free from the most abundant Os tri-oxide species (^{16}O$_3$),

311 allows the O isotope compositions to be determined by stripping masses 240, 241 and 242 of the minor

312 tri-oxide interferences, such as ^{189}Os^{16}O^{18}O$_2^-$ and ^{190}Os^{17}O$_3^-$ for mass 240. This will then provide the

313 signal intensity of only ^{192}Os^{16}O$_3^-$, ^{192}Os^{16}O$_2^{17}$O$^-$, and ^{192}Os^{16}O$_2^{18}$O$^-$ on respective masses 240, 241, and

314 242. For this first step of oxygen corrections we used the O$_{gas}$ isotope composition as determined by

315 Luguet et al. (2008)[37]. The ^{18}O/^{16}O was then calculated from the "stripped" 242/240 ratio and the

316 ^{17}O/^{16}O ratio could be determined from the "stripped" 241/240 ratio. However, as discussed in more

317 detail in section 4.2.2.1, in this study ^{17}O/^{16}O ratios were inferred using ^{18}O/^{16}O ratios. The oxygen

318 correction is described in detail in the Electronic Supplementary Information.

319 Due to the presence of isobaric Os oxide complexes, additional steps in the data reduction

320 compared to MC-ICP-MS were required. We adopted the following sequence of corrections; abundance

321 sensitivity (0.3 ppm[37]), a preliminary oxide isotope composition correction, PtO$_2^-$ and ReO$_3^-$ interference

322 corrections, a second O isotope composition correction, and double spike deconvolution (see section

323 4.1.2). The first O interference correction is solely used to correct for O isobaric interferences on PtO$_2^-$.

324 Subsequently, the PtO$_2^-$ interference corrected ^{184}OsO$_3^-$ and ^{186}OsO$_3^-$ values were used in the second O

325 correction. For isobaric PtO$_2^-$, WO$_3^-$ and ReO$_3^-$ interference corrections, the ion counter measurement

326 routines (before and after) were utilized, assuming a linear behaviour throughout the main run. Using

327 a linear extrapolation is a simplistic approach but can be justified by the minor variation in beam

328 intensities between the two SEM runs in combination with the minor influence the interference

329 corrections have on the Os isotopic ratios (see section 4.2.2.2). The abundance sensitivity was assumed

330 to be similar to that determined by Luguet et al. (2008)[37].

331

4.2.2.1 Effect of the oxygen isotopic composition

332

The accuracy of the deconvolved δ^{190}Os value as well as of the radiogenic isotopic ratios is dependent

333

on the accurate determination of the O isotopic compositions (i.e. ^{17}O/^{16}O and ^{18}O/^{16}O) that are used

334

for O interference corrections.

335

The average ^{18}O/^{16}O ratios of individual double spiked DROsS analyses range between

336

0.002007 and 0.002050, a variation of 21 ‰, for analyses with a total Os beam intensity of >1 V. This

337

variation is comparable with that reported by previous Os studies by N-TIMS (e.g. Liu et al., 1998[53] – 30

338

‰; Luguet et al., 2008[37] – 14 ‰; Chatterjee and Lassiter, 2015[39] – 31 ‰; Chu et al., 2015[54]– 22 ‰). If

339

the ^{18}O/^{16}O ratio varies by 21 ‰, and the ^{17}O/^{16}O relationship is changed accordingly along a TFL, then

340

the absolute δ^{190}Os value will shift by ±0.11 ‰. For the ^{187}Os/^{188}Os and ^{186}Os/^{188}Os ratios the resulting

341

absolute shift is about ±20 ppm and ±25 ppm, respectively. It is, therefore, of high importance to

342

determine the specific oxygen isotopic composition of an analysis. When ^{total}Os beam intensities are on

343

average >1 V (>1.3 mV on mass 242), the difference in ^{18}O/^{16}O ratios between the first and last 20 cycles

344

of an individual run ranges, apart from two samples at -12 ‰, between +5 ‰ and -7 ‰, and is on

345

average -1.1 ‰. This is similar to the variation observed by Chatterjee and Lassiter (2015)[39]. Larger

346

variations are observed for measurements made at lower beam intensities and the variability appears

347

to be more substantial when samples are run over a longer time period (Fig. 4). If the ^{18}O/^{16}O ratio is

348

changed by ±7 ‰, the absolute composition of δ^{190}Os shifts by ±0.025 ‰. The ^{187}Os/^{188}Os and

349

^{186}Os/^{188}Os ratios are shifted by ±11 ppm and ±26 ppm, respectively. We, therefore, suggest

350

determining the oxygen isotopic composition for each individual cycle, as this is the only way by which

351

small time scale variations throughout the run can be monitored and controlled.

352

Run-specific ^{17}O/^{16}O ratios for each individual cycle can either be measured directly, using

353

mass 241, or can be calculated based on the ^{18}O/^{16}O ratios. We will first consider the measured ^{17}O/^{16}O

354

ratios. For DROsS analyses, the average measured ^{17}O/^{16}O ratio was found to display a large variation,

355

of 121 ‰, with values ranging from 0.000369 to 0.000419. When only considering analyses with total

356

beam intensities of >1 V the ^{17}O/^{16}O ratios vary between 0.000369 and 0.000395, 66 ‰. Analyses with

357

an anomalously high or low ^{17}O/^{16}O ratio yield inaccurate δ^{190}Os values as well as ^{187}Os/^{188}Os and

358

^{186}Os/^{188}Os ratios, and show a positive correlation with ^{17}O/^{16}O (R^2 of 0.78, 0.78 and 0.76 respectively;

359

Fig. 5a-c). Anomalous values are only obtained for analyses performed at low beam intensities (Fig. 5d-

360

f). In contrast, the measured ^{18}O/^{16}O ratios do not show any co-variation with Os isotopic compositions

361

(R^2=0.28) suggesting that the inaccuracy on the Os isotopic compositions is dominantly introduced by

362

the ^{17}O/^{16}O ratio. Mass 241 has been measured at very low beam intensities (<5 mV) that are, in general,

363

5.2 times lower than for mass 242. The determination of ^{17}O/^{16}O is, therefore, more sensitive to

364

inaccuracies introduced by small variations in the instrument baseline occurring during an analysis.

365

Including more and longer baselines with longer integration times during an analysis would enhance

366

the accuracy of the baseline and potentially improve the measurement of the ^{17}O/^{16}O ratio.

367

368   Incorporation of 10^{12} Ω or 10^{13} Ω resistors to collect mass 241 and 242 would also be advantageous,

369   although these were not explored in this study.

370   The inaccuracy introduced by the measured $^{17}O/^{16}O$ ratio can be eliminated by calculating the

371    $^{17}O/^{16}O$ from the measured $^{18}O/^{16}O$ ratio. We will refer to this as the "calculated" $^{17}O/^{16}O$ ratio.

372   Recently, a similar approach has been used for N-TIMS isotope measurements of Mo[52], Ru[55], and W[56].

373   In this study, we assume that the oxygen isotopic compositions vary as a result of equilibrium mass-

374   dependent isotopic fractionation along a "Terrestrial Fractionation Line" (TFL[57]). For natural samples

375   the relationship between $\delta^{17}O$ and $\delta^{18}O$, when considered in logarithmic space, typically varies between

376   0.524-0.528 [e.g.58-60]. We have taken an average of the published values, 0.526, which translates to an

377   approximately linear slope of 0.0994 x + 0.000183, where x is $^{18}O/^{16}O$, over a $^{18}O/^{16}O$ interval of

378   0.002007 to 0.002055, the range in $^{18}O/^{16}O$ as observed for analyses in this study. Figure 6 shows that

379   the measured oxygen compositions of double spiked DROsS analyses with a total Os beam intensity of

380   >2 V closely plot along this line. Details of calculation $^{17}O/^{16}O$ from the measured $^{18}O/^{16}O$ are provided

381   in the supplementary information.

382   The resulting calculated $^{17}O/^{16}O$ ratios display a much smaller variation of 20 ‰ with values

383   ranging between 0.000383 and 0.000390, and is 10 ‰ when only considering analyses of >1 V. No

384   residual correlation between calculated $^{17}O/^{16}O$ ratios and Os isotopic compositions is observed

385   anymore (Fig. 5a-c). However, with decreasing beam intensities the $\delta^{190}Os$ values display a preferential

386   drift towards heavier values (up to 0.11‰) instead of showing a normal distribution (Fig. 5d). The

387    $^{187}Os/^{188}Os$ and $^{186}Os/^{188}Os$, on the other hand, drift preferentially towards lower values although higher

388   values are observed as well (Fig. 5e,f). When the calculated instead of the measured $^{17}O/^{16}O$

389   composition is used, the long-term reproducibility of $\delta^{190}Os$ is improved from 0.106 ‰ to 0.046 ‰ (2

390   sd; $n = 94$), and from 0.059 ‰ to 0.029 ‰ for analyses of >1 V ($n = 83$). For the remainder of this paper,

391   we will only consider analyses with a $^{total}Os$ beam intensity of >1 V, equivalent to, in general, >1.3 mV

392   on mass 242 and >0.35 V on mass 236. The total Os signal intensity obtained for a certain quantity of

393   Os loaded is highly variable, but is typically >1 V for loads of ≥2.3 ng natural Os.

394

395   *4.2.2.2 Effect of polyatomic interferences*

396   The interference intensities monitored on masses 228, and 230-233 in this study are comparable to

397   those reported by Luguet et al. (2008)[37]. Beam intensities on mass 228 (predominantly $^{196}Pt^{16}O_2^-$)

398   ranged from 12,000 – 1,400,000 cps (counts per second) which relates to a potential $^{196}Pt^{18}O_2^-$

399   interference of 0.05-6 cps on mass 232 (predominantly $^{184}Os^{16}O_3^-$). For mass 230 (mainly $^{198}Pt^{16}O_2^-$)

400   intensities ranged between 4,000-1,050,000 cps which results in respective interferences of 16-4,300

401   cps and 0.02-4.4 cps on masses 232 ($^{184}Os^{16}O_3^-$) and 234 ($^{186}Os^{16}O_3^-$). The PtO_2^- interference on mass 234

402   is negligible, whereas the combined PtO_2^- interferences on mass 232 reached a maximum of 4,306 cps.

403   This represents 2.5 % of the typical total signal at mass 232 which can lower the $^{184}Os/^{188}Os$ substantially

404   (~30,000 ppm). In this study, mass 234 was only monitored to correct for polyatomic oxygen

405   interferences on the other Os isotopic ratios. Lowering the $^{184}Os/^{188}Os$ by 30,000 ppm results in a minor

406   shift of -2 ppm on the $^{186}Os/^{188}Os$ and has no noticeable effect on the other Os isotopic ratios. The

407   average difference between the two SEM runs, before and after the main run, was 250,000 cps for mass

408   228 and 135,000 cps for mass 230. Potential within-run variations of this magnitude have no

409   measurable effect on the isotopic ratios. On mass 231, $^{183}WO_3^-$, we obtained intensities of 6-1,000 cps,

410   which produce insignificant interferences on $^{186}Os^{16}O_3^-$ [37, 61]. Mass 233, $^{185}ReO_3^-$, displayed intensities

411   between 3-460 cps but were generally below 300 cps and on average 73 cps. Translated to $^{187}ReO_3^-$ this

412   means <502 cps or 8 μV that interfered on the $^{187}OsO_3^-$. Typically, this quantity equates to a lowering of

413   the $^{187}Os/^{188}Os$ by <100 ppm and on average 38 ppm, which is close to the 2 se of our measurements

414   (40 ppm) but much smaller than the long-term reproducibility (268 ppm; 2 sd). Between the pre- and

415   post SEM runs, the beam intensities on mass 233 generally varied by 33 cps which equates to a shift of

416   ~18 ppm on the $^{187}Os/^{188}Os$. To summarize, polyatomic interferences from PtO_2^-, WO_3^-, and ReO_3^-

417   monitored in this study had no noticeable effect on the stable Os and $^{186}Os/^{188}Os$ isotopic composition,

418   and were minor for $^{187}Os/^{188}Os$ ratios.

419

420   **5. RESULTS AND DISCUSSION**

421   Results are presented in Tables 4 and 5, and shown in Figures 7-13. All internal errors are quoted as 2

422   standard error (2 se), whereas short term (i.e. single session) and long-term (i.e. multiple sessions)

423   reproducibilities are given as 2 standard deviations (2 sd).

424

425   **5.1 Internal precision, external reproducibility and accuracy**

426   ***5.1.1 Stable osmium isotope ratios by MC-ICP-MS***

427   The internal precision (2 se; $n \le 80$ cycles, depending on 2 se outlier rejection) on a single $\delta^{190}Os$ MC-

428   ICP-MS analysis is typically between 0.01-0.02 ‰ when ^{188}Os beam intensities range between 7-4 V

429   (~18-11 V $^{total}Os$; Fig. 7). The amount of natural Os consumed is ~200 ng. The observed precision is in

430   good agreement with the theoretical error as calculated in section 2.1 (Fig. 7) suggesting that the model

431   considers all the errors that should be accounted for. Small deviations from the calculated error could

432   have arisen from, for example, variation in the spike – sample proportions, or the number of cycles

433   included. The model considers 80 cycles whereas this can be less for MC-ICP-MS if outliers are rejected.

434   This also explains why the error model for N-TIMS displays lower errors for a given intensity, as 280

435   cycles were considered for N-TIMS analyses.

436   Repeated analyses of reference standard solution DROsS, obtained during multiple analytical

437   sessions over a time period of ~22 months, show an external reproducibility on $\delta^{190}Os$ of 0.016 ‰ (2

438   sd; n = 91; Fig. 8; Table 4). The short-term reproducibility of a single analytical session when consuming

439   ~200 ng natural Os at total beam intensities of 11-18 V is 0.014-0.029 ‰ (2 sd; *n* = 2-10). A similar

440   precision and reproducibility is obtained for in-house Os reference solutions ROMIL, SpecPure and

441   OsCaR (Fig. 7 and 9; Table 4). As this study is the first to present stable Os isotope compositions, the

442   accuracy cannot be assessed by measurement of pre-calibrated reference materials. Instead we have

443   performed standard-sample bracketing measurements by MC-ICP-MS using natural (i.e. non DS)

444   reference solutions. Comparison of this technique with the DS method shows that a similar offset

445   between DROsS and the other Os reference solutions is obtained (Fig. 9; Table 4) which is in support of

446   the relative accuracy of our method.

447

448   *5.1.2 Stable osmium isotope ratios by N-TIMS*

449   For a single δ^{190}Os analysis by N-TIMS the internal precision (2 se; n ≤ 280 cycles, depending on 2 se

450   outlier rejection) ranges between 0.010-0.040 ‰ when ^{188}OsO$_3^-$ beam intensities vary from 6-0.43 V

451   (~18 to 1 V ^{tot}Os beam; Fig. 7). These intensities were obtained for load sizes between 45 and 2.3 ng

452   natural Os. Repeated analyses of double spiked reference solution DROsS, over approximately 22

453   months, yield an external reproducibility on δ^{190}Os of 0.029 ‰ (2 sd; *n* = 83; Fig. 8; Table 4). The majority

454   of these analyses (*n* = 44) comprised a load of 10-20 ng natural Os, 20 analyses had a load of >20 ng,

455   and 19 analyses were performed with less than 10 ng Os. That DROsS yields less precise and less

456   reproducible results for N-TIMS than MC-ICP-MS is, predominantly, a consequence of the lower beam

457   intensities at which the analyses were performed. Analyses of in-house pure Os solutions ROMIL,

458   SpecPure and OsCaR show a similar precision and reproducibility (Fig. 7 and 9; Table 4). That ROMIL

459   and SpecPure display a similar offset relative to DROsS for N-TIMS as for MC-ICP-MS analyses provides

460   support to the accuracy of our method.

461

462   *5.1.3 Radiogenic isotope ratios by MC-ICP-MS*

463   The precision that can be obtained for ^{187}Os/^{188}Os and ^{186}Os/^{188}Os isotopic ratios is <100 ppm (2 se; n ≤

464   280 cycles, depending on 2 se outlier rejection) when ^{187}Os and ^{186}Os average beam intensities are

465   higher than ~0.06 V over the ~11 minutes of the analysis. When average beam intensities of >0.18 V

466   are achieved this improves to ~40 ppm (Fig. 7). This is comparable with the precisions reported by

467   Nowell et al. (2008; <40 ppm at high signal intensities)[36] and corresponds with the errors predicted by

468   the model described in section 2.1 (30-40 ppm at 0.22 V; Fig. 7). Repeated analyses of double spiked

469   reference standard DROsS yields a reproducibility of 123 and 138 ppm for ^{187}Os/^{188}Os and ^{186}Os/^{188}Os,

470   respectively (2 sd, *n* = 91). This is higher than that reported by Nowell et al. (2008)[36] for DROsS (19 ppm)

471   but is comparable with the long-term reproducibilities reported for reference materials UMd (220 ppm

472   for ^{187}Os/^{188}Os and 108 ppm for ^{186}Os/^{188}Os) and DTM (149 ppm for ^{187}Os/^{188}Os and 67 ppm for

473   ^{186}Os/^{188}Os).

474   For radiogenic isotopic ratios we can use previous studies to assess the accuracy of our

475   method. In addition, we have compared double spiked data with that from unspiked runs, and used

476   DROsS for un-spiked sample-standard bracketing measurements. We have applied these methods to

477   DROsS as well as to pure Os solutions ROMIL, SpecPure, and OsCaR. Taken together, the various samples

478   encompass a significant range in $^{187}Os/^{188}Os$ isotopic ratios over which to test our analytical methods.

479   Table 4 shows that all values obtained in this study, using the various methods, are within analytical

480   uncertainty with one another as well as with previously published values of un-spiked DROsS

481   measurements.[36, 37]

482

483   *5.1.4 Radiogenic isotope ratios by N-TIMS*

484   For N-TIMS analyses the internal precision on both $^{187}Os/^{188}Os$ and $^{186}Os/^{188}Os$ is <100 ppm (2 se; n ≤

485   280 cycles, depending on 2 se outlier rejection) for analyses with average $^{187}OsO_3^-$ and $^{186}OsO_3^-$ beam

486   intensities >0.03 V over the 280 cycles of analysis, and improves to <40 ppm at high signal intensities

487   (>0.18 V; Fig. 7). This is slightly greater than the precisions reported by Luguet et al. (2008[37]; <30 ppm

488   at >0.08 V). Repeated analyses of reference standard DROsS yield a reproducibility of 268 ppm and 361

489   ppm for $^{187}Os/^{188}Os$ and $^{186}Os/^{188}Os$ ratios, respectively (2 sd, *n* = 83) for loads varying between 2.3 and

490   45 ng natural Os. This is significantly higher than the values reported by Luguet et al. (2008[37]; 26 and 48

491   ppm, respectively). Where Luguet et al. (2008)[37] have only included analyses with $^{187}OsO_3^-$ and $^{186}OsO_3^-$

492   beam intensities of 80 mV or above we have taken analyses with intensities down to 20 mV into

493   account. When excluding the analyses with beam intensities <80 mV on $^{187}OsO_3$- and $^{186}OsO_3$- we obtain

494   a long-term reproducibility of 90 and 89 ppm, respectively (2 sd; *n* = 22). These slightly higher analytical

495   uncertainties are related to error propagation inherent in double-spike deconvolution. That errors are

496   higher than predicted by the model is, predominantly, because the error on the oxygen composition

497   was not incorporated in the model, whereas it has been propagated for the actual analyses.

498   To assess the accuracy, we have compared the radiogenic values obtained by our DS method,

499   with those determined for unspiked runs, and with previous studies (Table 4). All values are within

500   analytical uncertainty of one another which demonstrates that our method is able to obtain accurate

501        $^{187}Os/^{188}Os$ and $^{186}Os/^{188}Os$ isotopic ratios by N-TIMS. This provides a valuable quality control on the DS

502   calculations and allows the acquisition of both the stable and radiogenic isotope composition within a

503   single analytical run.

504

505   **5.2. Geological materials**

506   During the course of this study, we have measured four international geological reference materials.

507   The selected materials cover a range of matrices; (1) UB-N[40], a serpentinised and fertile lherzolite from

508   the Voges in France; (2) GP-13[41, 62], a fertile lherzolite from the Beni Bousera massif in Morocco; (3)

509   CHR-Bkg [42, 43] and (4) CHR-Pt+[42, 63], which are both chromitites from the Shetland ophiolite in Scotland,

510 UK. Furthermore, we have analysed the ordinary H-chondrite Zag. Although this is not an international

511 reference material, sufficient sample material was available to perform several replicate analyses

512 allowing the exploration of another type of sample matrix. Stable and radiogenic Os isotope

513 compositions, together with Os abundances, are given in Table 5 and shown in Fig. 10-13.

514

5.2.1 Radiogenic osmium isotope compositions for geological materials

516 We have shown that double spiked DROsS analyses display $^{187}Os/^{188}Os$ and $^{186}Os/^{188}Os$ ratios consistent

517 with previous published studies, and that ROMIL and SpecPure yield similar values for various methods

518 (i.e. non-DS, DS, standard sample bracketing). This means that although the main aim of this method is

519 to obtain high precision stable isotope data it also has the potential to provide radiogenic isotopic ratios

520 within the same analyses. This is particularly beneficial when dealing with limited amounts of available

521 sample material that only allows a single analysis. Furthermore, it significantly reduces processing and

522 measurement time.

523   Apart from three UB-N analyses, all data is obtained at average $^{187}OsO_3^-$ and $^{186}OsO_3^-$ beam

524 intensities of ≥0.01 V for N-TIMS ($^{total}Os$ ≥ 1 V) analyses and ^{187}Os and ^{186}Os ≥0.03 V for MC-ICP-MS

525 ($^{total}Os$ ≥ 1 V). The influence of the $^{17}O/^{16}O$ composition and OPZ on the accuracy of the isotopic

526 compositions is shown to be negligible at these intensities. Geological materials analysed in this study

527 display $^{187}Os/^{188}Os$ values that are consistent with the range of values obtained by previous studies (Fig.

528 10 and 13). However, a significant degree of irreproducibility (up to 7,400 ppm) can be observed which

529 will be discussed below. The variability observed for $^{186}Os/^{188}Os$ ratios is much smaller, 251-537 ppm,

530 and comparable with the long-term reproducibility obtained for N-TIMS DROsS analyses (361 ppm). The

531 $^{186}Os/^{188}Os$ ratios of all samples range from 0.119746 ± 42 to 0.119856 ± 47, which is in close

532 approximation of the upper mantle value (0.119837±5)[64] but consistently lower (Fig. 11). Assessment of

533 the accuracy of our $^{186}Os/^{188}Os$ values by direct comparison with previously published values for these

534 samples is not possible as they have not been measured for $^{186}Os/^{188}Os$ before. At this point, the reason

535 for the lower values is unclear and further investigation is required.

536

5.2.2 Stable osmium isotope compositions for geological materials

538 The internal precision and external reproducibility on $\delta^{190}Os$ are similar to that obtained for pure Os

539 isotope solutions. One exception is the reproducibility reported by CHR-Pt+. This will be discussed in

540 more detail in the next section. Similar to Os standard solutions, replicate analyses of chondrite ZAG

541 show similar values for MC-ICP-MS and N-TIMS analyses, providing further support for the accuracy of

542 our method on a real sample matrix.

543   All reference materials are derived from Earth's mantle. The materials show no resolvable

544 variation at the 95 % c.i. level and provide an average $\delta^{190}Os$ value of 0.130 ± 0.032 ‰ (2 sd; n = 4). The

545 geological reference material CHR-Bkg displays the lightest composition of δ^{190}Os = 0.124 ± 0.020 ‰ (2

546 sd; n = 7) and chromitite CHR-Pt+ the heaviest at 0.162 ± 0.051 (2 sd; n = 4). Ordinary chondrite Zag

547 yields a δ^{190}Os value of +0.123 ± 0.018 ‰ (2 sd; n = 9) which is indistinguishable, within uncertainty,

548 from the mantle derived samples.

549   Interestingly, DROsS is the only material that displays a different, isotopically lighter,

550 composition relative to the other materials measured in this study. This offset could (a) be a product of

551 the chemical extraction of Os from the source material, or (b) reflect the original composition of the

552 material the Os was sourced from.

553

554 ***5.2.3 Effect of sample digestion***

555 In mantle rocks, osmium is concentrated in refractory accessory phases that are heterogeneously

556 distributed throughout the rock (the "nugget" effect). This has led to difficulties in repeating results

557 when considering Os abundances and ^{187}Os/^{188}Os ratios. Over the past two decades, various digestion

558 methods have been assessed in order to resolve this problem [e.g. 40, 44, 65, 66]. Acid attack digestions using

559 sealed glass Carius tubes (CT[23, 45]) and the high-pressure asher system (HPA[44]) are most frequently used.

560 This is because they are considered to be most efficient in attacking the highly resistant phases that are

561 likely to contain appreciable Os (such as Cr-spinel and platinum-group minerals). In this study, we have

562 applied both techniques to various geological materials. A limitation of both techniques is the maximum

563 amount of sample material that can be digested effectively (≤2 g). In the case of geological samples

564 with low Os abundances (e.g. most mantle material like UB-N, and nearly all crustal material) more than

565 2 g of material is needed to obtain high precision data. To circumvent this problem, we have digested

566 several sample aliquots of UB-N and GP-13, and combined them prior to solvent extraction. As for the

567 individual processed samples, each aliquot was spiked before digestion. As the proportion of spike is

568 one of the unknowns calculated during the resolution of the DS equation system, it should be noted

569 that reaching a 100 % yield across all aliquots during sample processing is not required to generate

570 accurate isotope ratios and concentration determinations, providing that spike-sample equilibration

571 occurs before loss of any Os during sample processing.

572   Apart from CHR-Pt+, replicate digestion of individual samples shows no detectable stable

573 isotope variation and no systematic difference between CT or HPA digestions. For the combined

574 aliquots of UB-N, relative to the single digestions, we do not observe any variation for stable Os isotopes

575 either (Fig. 12; Table 5). The two analyses of combined GP-13 aliquots show consistent stable isotope

576 compositions. By contrast, statistically resolvable variations in ^{187}Os/^{188}Os ratio and Os abundance were

577 observed in all the samples tested. In the case of UB-N and CHR-Bkg, ^{187}Os/^{188}Os is positively correlated

578 with 1/[Os] (Fig. 13). This co-variation was observed previously, in a more extensive study of UB-N, by

579 Meisel et al. (2003)[40]. The CHR-Bkg analyses reported within that study display a more limited variation

580 and no significant co-variation between Os abundance and radiogenic isotopic composition was

581   discussed. If we incorporate the CHR-Bkg data of Meisel et al. (2003)[40] they fall within the trend

582   obtained in this study. The observed variation in radiogenic isotopes can be explained by incomplete

583   digestion and/or sample heterogeneity. In both cases this indicates that within the digested material

584   different phases, or phases of different generations, possess distinct radiogenic isotopic composition.

585   The absence of stable Os isotope variation, for these particular aliquots, implies that there is no

586   significant difference in stable isotope composition of the phases in these samples. As such, the type of

587   digestion technique, or the combination of individual digestions, appears to have no influence on the

588   stable isotope composition for these particular samples.

589   For CHR-Pt+ we observe a larger range in stable Os isotope compositions (δ^{190}Os = +0.129 –

590   0.198 ‰), which is reflected in the relatively poor reproducibility (0.051‰). The stable isotope data

591   appear to co-vary with Os abundance, with the heavier values corresponding to higher Os abundance

592   of 17.5 % (Fig. 12). As discussed before, variance in isotopic composition correlating with Os abundance

593   may indicate that phases within the whole rock contain different stable isotopic signatures. Our

594   preliminary data suggests that phases within chromitite CHR-Pt+ possess different stable Os isotopic

595   compositions. Previous studies that focused on the origin of chromitites derived from the Cliff deposit

596   in the Shetland Ophiolite concluded that initial PGE concentrations were caused by magmatic processes

597   followed by a hydrothermal overprint which locally remobilized and re-concentrated the PGE.[67] This

598   secondary process might be the source of Os stable isotope fractionation, but further investigation is

599   required.

600

601   **6. CONCLUSIONS**

602   We have developed a method for high-precision measurement of stable Os isotope compositions by

603   both plasma source (MC-ICP-MS) and thermal ionisation mass spectrometry (N-TIMS). The method

604   utilizes a ^{188}Os-^{190}Os double spike that is added to the sample prior to digestion with a spike-sample

605   proportion of 0.55:0.45. We show that the technique is robust when dealing with matrix effects and

606   interference corrections on MC-ICP-MS, even for levels up to 10 % of the total Os concentration, and

607   that the memory effect for MC-ICP-MS analyses is negligible. Analyses performed by N-TIMS show that

608   the oxygen isotopic composition exerts a major control on the accuracy of the isotopic ratios. It is

609   suggested that the oxygen isotopic composition is obtained for every specific run, by measuring the

610   ^{18}O/^{16}O for each individual cycle, and calculating the ^{17}O/^{16}O ratio from the ^{18}O/^{16}O ratio, especially

611   when the total Os signal intensity drops below 2 V.

612   The internal precision (2 se) on the δ^{190}Os measurement (permil difference of the ^{190}Os/^{188}Os

613   ratio relative to reference standard DROsS) of a single analysis is 0.010-0.025 ‰ for MC-ICP-MS (~200

614   ng natural Os; n = 80 cycles) and 0.010-0.030 ‰ for N-TIMS (2.3-45 ng natural Os; n = 280 cycles). The

615   long-term reproducibility of reference material DROsS is 0.016 ‰ (2 sd; n = 91) and 0.029 ‰ (2 sd; n =

616   83) for MC-ICP-MS and N-TIMS, respectively.

617   The method is shown to be capable of obtaining Os stable isotope compositions of terrestrial
618   and extra-terrestrial materials with a high precision and reproducibility. The first data obtained for
619   geological materials are all within analytical uncertainty of one another, despite the measurement of
620   samples reflecting a range of source regions, chemical compositions, geological history, and radiogenic
621   isotope ratios. Minor variations between different digestions of chromitite CHR-Pt+ hints at Os stable
622   isotope fractionation as a result of Os remobilization due to hydrothermal alteration. Overall, our
623   preliminary δ^{190}Os value for the Earth's upper mantle is +0.130 ± 0.032 ‰ (2 sd; n = 4), which is
624   indistinguishable from a value of +0.123 ± 0.018 ‰ (2 sd; n = 9) obtained for the ordinary H-chondrite
625   Zag.

626

634

635

FIGURE CAPTIONS

637 **Figure 1** Results for an error (2 se) simulation on the stable isotope composition in ‰ amu^{-1} in case of a ^{188}Os-^{190}Os
638 double spike. The red dot indicates that minimal error propagation of ~0.010 ‰ amu^{-1} (2 se) is obtained when
639 using a 60 % ^{188}Os – 40 % ^{190}Os spike that is mixed with a sample in relative proportions of 55 % and 45 %. Note
640 that errors are minimal (<0.020 ‰ amu^{-1}) over a large range of sample-spike mixtures (15 – 81 % sample fraction).
641 The error model is based on the method of Millet and Dauphas (2014)[33] using the following parameters: 6 V; 80 x
642 8.3 sec integrations; 10^{11} Ω collectors; T= 290 K.

643 **Figure 2** Results of double spiked DROsS analyses measured using MC-ICP-MS (closed symbols) at variable beam
644 intensities to assess the effect of beam intensity and the on-peak zero on the accuracy of the δ^{190}Os and ^{187}Os/^{188}Os
645 composition. Data show that all measurements display δ$^{190/188}$Os and ^{187}Os/^{188}Os compositions within analytical
646 uncertainty of the long-term reproducibility as determined for >10 V analyses. The black dotted line indicates the
647 average DROsS value, as obtained from the >10 V analyses, with the ±2 sd represented by the grey band.

648 **Figure 3** Results of doping tests to assess the robustness of the method against residual matrix effects on the MC-
649 ICP-MS. Data show that all measurements display δ$^{190/188}$Os compositions within analytical uncertainty of undoped
650 DROsS analyses for residual element abundances up to 10 % of the total Os concentration. The percentages indicate
651 the presence of each named element at x% of the Os abundance, e.g. Si was present at 5% of the Os abundance.
652 The black dotted line indicates the average DROsS value with the ±2 sd represented by the grey shaded band as
653 obtained in this study. Lith = lithophile elements (Si, Al, Mg, Fe, Ca, Ti, Ni, and Cr); PGE = Platinum Group Elements
654 (Ru, Rh, Pd, Ir, and Pt).

655 **Figure 4** The difference in measured ^{18}O/^{16}O ratios between the first and the last 20 cycles of double spiked DROsS
656 analyses (green circles) show an average variability of -1.1 ‰ (green dotted line). For clarity, two values with a
657 deviation of -12 ‰, at 1.4 V and 1.7 V, are excluded. The variability is shown to increase with decreasing beam
658 intensity and seems to be larger when samples are run twice for 280 cycles. Open symbols represent analyses
659 where the oxygen composition has been measured before and after the main run.

660 **Figure 5** Residual correlation for double spiked DROsS analyses by N-TIMS between the measured ^{17}O/^{16}O (grey
661 circles) and Os isotopic compositions; (a) δ$^{190/188}$Os, (b) ^{187}Os/^{188}Os, and (c) ^{186}Os/^{188}Os. No residual correlation is
662 observed when the ^{17}O/^{16}O is calculated from the measured ^{18}O/^{16}O ratio (green circles). The offset from the
663 expected DROsS value is seen to increase with decreasing beam intensities (d-f), with a reduced offset when using
664 calculated ^{17}O/^{16}O ratios. With decreasing signal intensity, (d) δ$^{190/188}$Os values seem to slightly drift towards
665 heavier values, and (e) ^{187}Os/^{188}Os and (f) ^{186}Os/^{188}Os towards lower values. The black dashed line represents the
666 expected DROsS value.

667 **Figure 6** Measured ^{18}O/^{16}O vs. ^{17}O/^{16}O ratios for DROsS analyses run at a total Os beam intensity of >2 V closely
668 follow the Terrestrial Fractionation Line (TFL). Analyses are divided based on the beam intensity on mass 242 (<5
669 mV; 5-10 mV; >10 mV). The TFL was calculated using a slope of 0.526 which translates to an roughly linear slope of
670 0.0994 x + 0.000183, where x is ^{18}O/^{16}O, over a ^{18}O/^{16}O interval of 0.002007 to 0.002055, the range in ^{18}O/^{16}O
671 obtained in this study. Also shown are oxygen isotope ratios from N-TIMS measurements in previous studies: Nagai
672 and Yokoyama (2016)[51]; Worsham et al. (2016) [52]; Luguet et al. (2008)[37]; Griselin et al. (2001)[68]; Chavagnac (1998)[69];
673 Thirlwall (1991)[70]; Reisberg and Zindler (1986)[71]; Nyquist in Wasserburg et al. (1981); Wasserburg et al. (1981)[72];
674 Nier (1950)[73].

675 **Figure 7** The analytical precision (2 se) on (a) δ$^{190/188}$Os and (b) ^{187}Os/^{188}Os plotted against the average (a) ^{188}OsO$_3$$^-$
676 and (b) ^{187}OsO$_3$$^-$ beam intensity (V) for analyses of reference material DROsS, and other pure Os solutions by MC-
677 ICP-MS or N-TIMS. The dashed (MC-ICP-MS) and dotted (N-TIMS) lines in (a) indicate the modelled error calculated
678 using the method of Millet and Dauphas (2014)[33] using the following parameters: 80 x 8.3 seconds integrations for
679 MC-ICP-MS and 280 x 8.3 seconds for N-TIMS; 10^{11} Ω collectors; T= 290 K. Note that the lower theoretical error for
680 N-TIMS results from the larger amount of cycles incorporated.

681 **Figure 8** Repeated analyses of reference material DROsS on both MC-ICP-MS (squares) and N-TIMS (circles)
682 obtained during multiple analytical sessions over a time period of 22 months. Analyses have been organized on
683 beam intensity, note that N-TIMS analyses are obtained at lower beam intensities. Sample size is approximately

684   200 ng natural Os for MC-ICP-MS and ranges between 2.3 and 45 ng natural Os for N-TIMS measurements, with
685   ^{total}Os beam intensities of >4 V for MC-ICP-MS analyses and >1 V for analyses by N-TIMS. Error bars quote the 2 se
686   error on the individual analysis, the grey band represents the ±2 sd of all analyses. Symbols in yellow correspond
687   to the annotated beam intensity.

688   **Figure 9** The $\delta^{190/188}$Os value obtained for repeat analyses of pure Os solutions ROMIL (triangle), SpecPure (circle)
689   and OsCaR (diamond) by both MC-ICP-MS (closed symbols) and N-TIMS (open symbols) obtained during the course
690   of this study. The striped, filled symbols indicate sample-standard bracketing data. All Os solutions show a similar
691   reproducibility as obtained for reference standard DROsS. Values obtained for ROMIL and SpecPure on MC-ICP-MS
692   and N-TIMS show values within analytical uncertainty supporting the accuracy of our method. The grey bands
693   indicate the reproducibility (±2 sd) obtained by MC-ICP-MS and N-TIMS. Error bars represent the 2 se error of an
694   individual analysis.

695   **Figure 10** The ^{187}Os/^{188}Os isotope ratios of geological materials UB-N, GP-13, CHR-Bkg, CHR-Pt+ and Zag analysed
696   by MC-ICP-MS (closed symbols) or N-TIMS (open symbols) display values consistent with previous studies (grey
697   bars). Literature data for maximum and minimum values: UB-N – ref. 40, 74; GP-13 – ref. 75, 76; CHR-Bkg – ref 40;
698   CHR-Pt+ - no previous published data; Zag – ref 3, 4.

699   **Figure 11** The ^{186}Os/^{188}Os ratios of geological materials UB-N, GP-13, CHR-Bkg, CHR-Pt+ and Zag analysed by MC-
700   ICP-MS (closed symbols) or N-TIMS (open symbols). Most samples plot below the upper mantle value of
701   0.119837±5 (2 sd; Ireland et al., 2011[64]). CT = Carius tube digestions, all other sample aliquots are processed using
702   the high-pressure asher system. * = an analysis for which digestions were combined prior to chemical Os extraction.
703   Error bars indicate the 2 se on the individual analysis.

704   **Figure 12** Osmium stable isotope compositions ($\delta^{190/188}$Os) of geological materials UB-N, GP-13, CHR-Bkg, CHR-Pt+
705   and Zag analysed by MC-ICP-MS (closed symbols) or N-TIMS (open symbols). Symbols are ordered from high to low
706   Os concentration. Apart from Zag, which is an ordinary chondrite, all samples are reference materials sourced by
707   the Earth's mantle. Symbols as in Fig. 11.

708   **Figure 13** Correlation between ^{187}Os/^{188}Os ratio and 1/[Os] for reference materials UB-N (circles) and CHR-Bkg
709   (triangles), as obtained for independently processed sample aliquots in this study (open symbols). Included are
710   data as obtained by Meisel et al. (2003[40]; filled symbols).

711

TABLE CAPTIONS

Table 1 Osmium isotopic ratios of reference standard DROsS, as determined by Nowell et al. (2008)[36] normalized
to $^{189}Os/^{188}Os$ to correct for mass bias, and of the ^{188}Os-^{190}Os double spike (DS) as used in this study. The quoted
error on DROsS represents the 2 sd on 21 analyses, and the error on the DS is the relative 2 se on the analysis used
to obtain the DS composition.
Table 2 Faraday cup configuration used for osmium isotope measurements by static multi-collection on a Thermo
Neptune MC-ICP-MS and Thermo Triton Plus N-TIMS at Durham University. Only principal ions measured are listed,
see ref. 37 (Luguet et al., 2008) for a full list of known polyatomic interferences.
Table 3 Osmium stable isotope compositions ($\delta^{190/188}Os$) of analytical tests on the MC-ICP-MS showing the
robustness of our methodology with regards to (i) signal intensity and (ii) matrix effects and interference
corrections. The percentages indicate the presence of each named element at x% of the Os abundance, e.g. Si was
present at 5 % of the Os abundance. *Lith = Lithophile elements (Si, Al, Mg, Fe, Ca, Ti, Ni, and Cr); **PGE = Platinum
Group Elements (Ru, Rh, Pd, Ir, and Pt).

Table 4 Average osmium stable and radiogenic isotope ratios of DROsS, SpecPure, ROMIL and OsCaR obtained in
this study using: the double spike (DS) method; sample-standard bracketing by MC-ICP-MS, using non DS solutions
and DROsS as the reference bracketing standard; and un-spiked runs by N-TIMS. For comparison the radiogenic
isotope composition of DROsS as obtained by previous studies is included (Nowell et al., 2008[36]; Luguet et al.,
2008[37]). Note that the better reproducibility (2 sd) for MC-ICP-MS relative to N-TIMS is, predominantly, related to
difference in beam intensities at which analyses have been made (11-18 V vs. 1-18 V total Os beam, respectively).
* - Four individual sample-standard bracketing sessions were run, on different days, and include 16 analyses all
together. Presented are the average and 2 sd on the averages of the four analytical sessions.

Table 5 Osmium stable ($\delta^{190/188}Os$) and radiogenic ($^{187}Os/^{188}Os$ and $^{186}Os/^{188}Os$) isotope compositions, and Os
abundances of geological materials obtained by either MC-ICP-MS or N-TIMS. Samples are digested using carius
tubes (CT) or the high-pressure asher (HPA) system. W. mean = weighted mean; * = aliquots of sample material
that are combined after digestion and prior to chemical separation of Os.

740 **FIGURES**

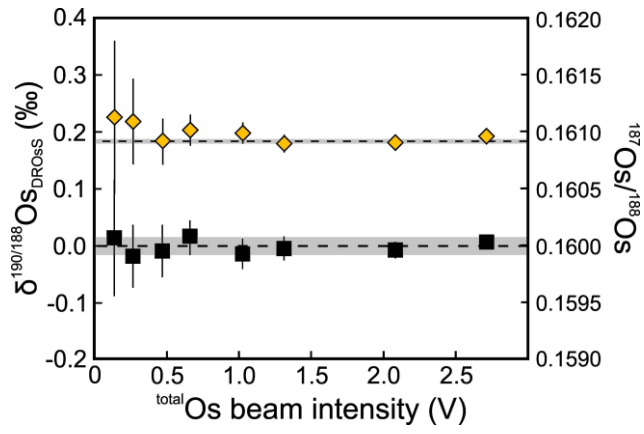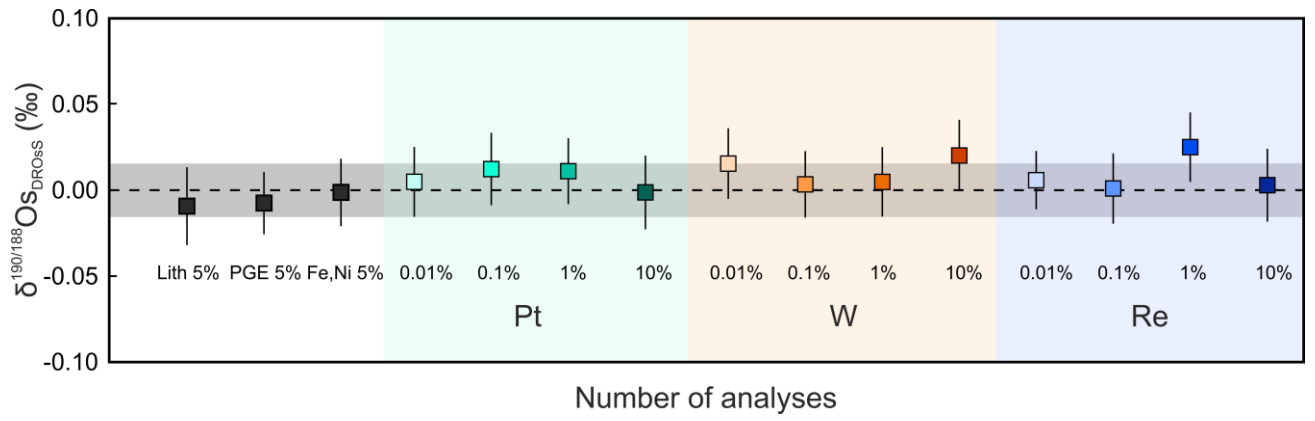741 **Figure 1**
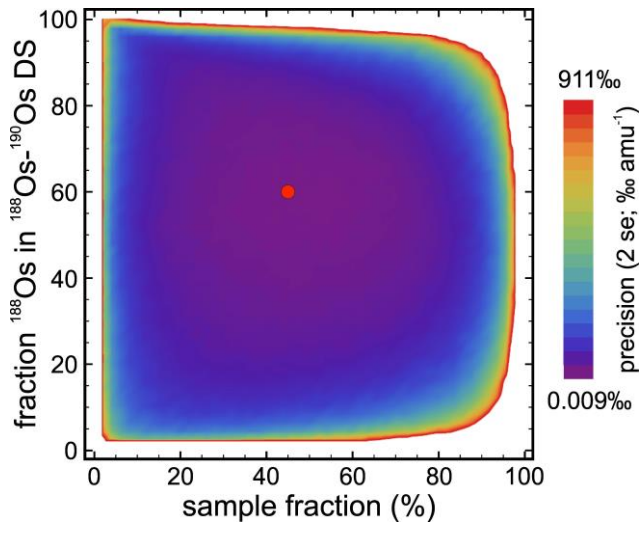
742

743   **Figure 2**

744

745 **Figure 3**

746

747 **Figure 4**

748
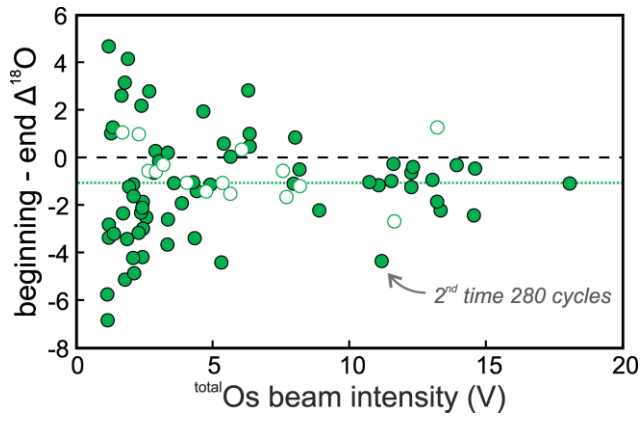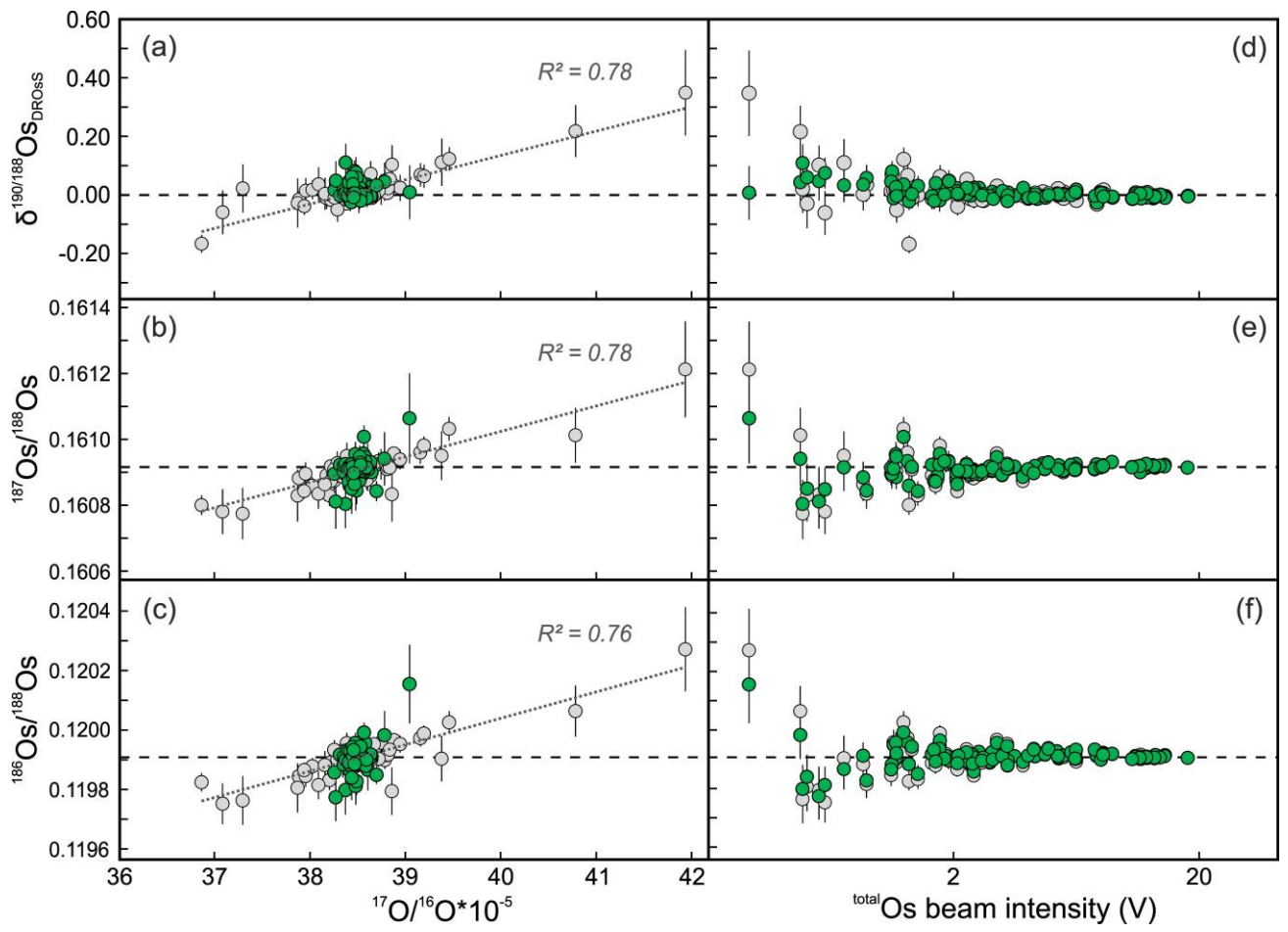
749 **Figure 5**
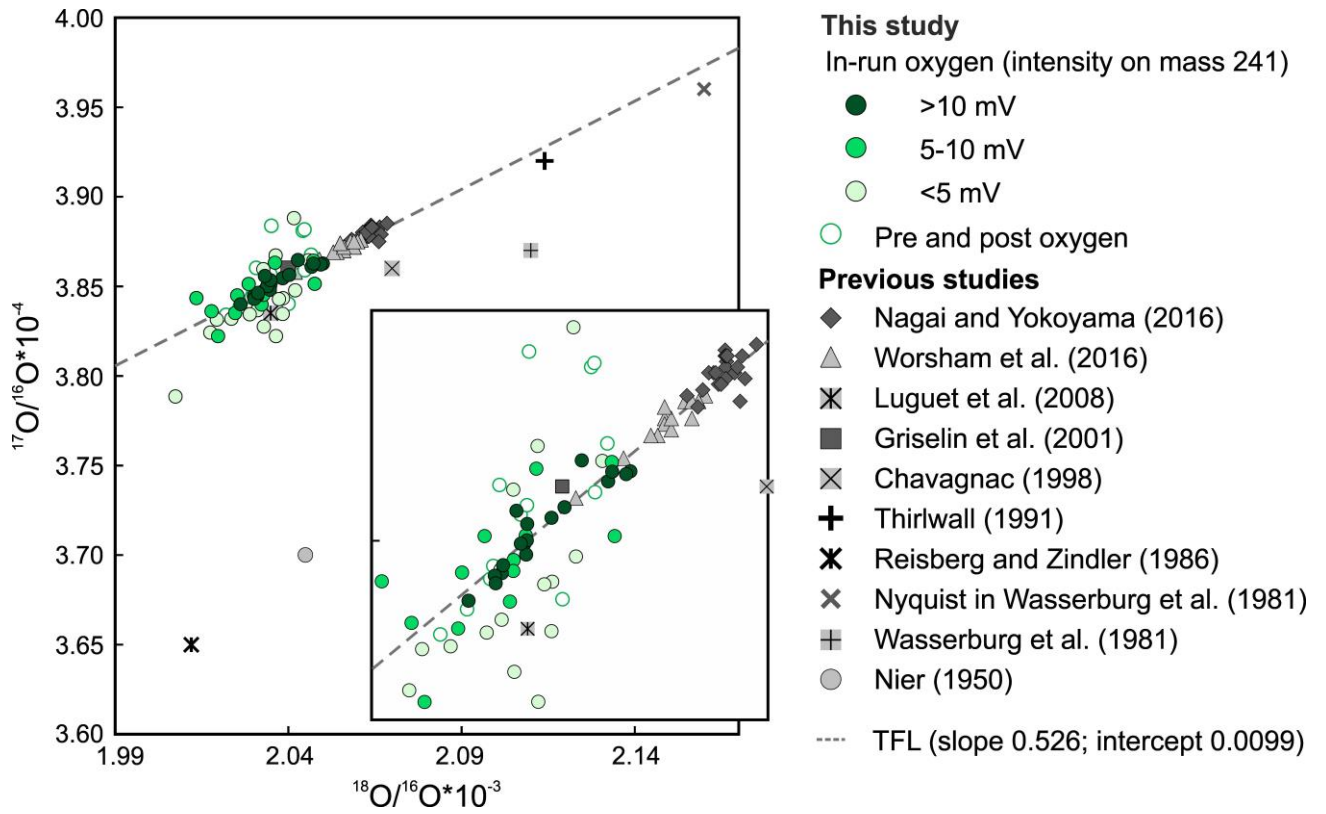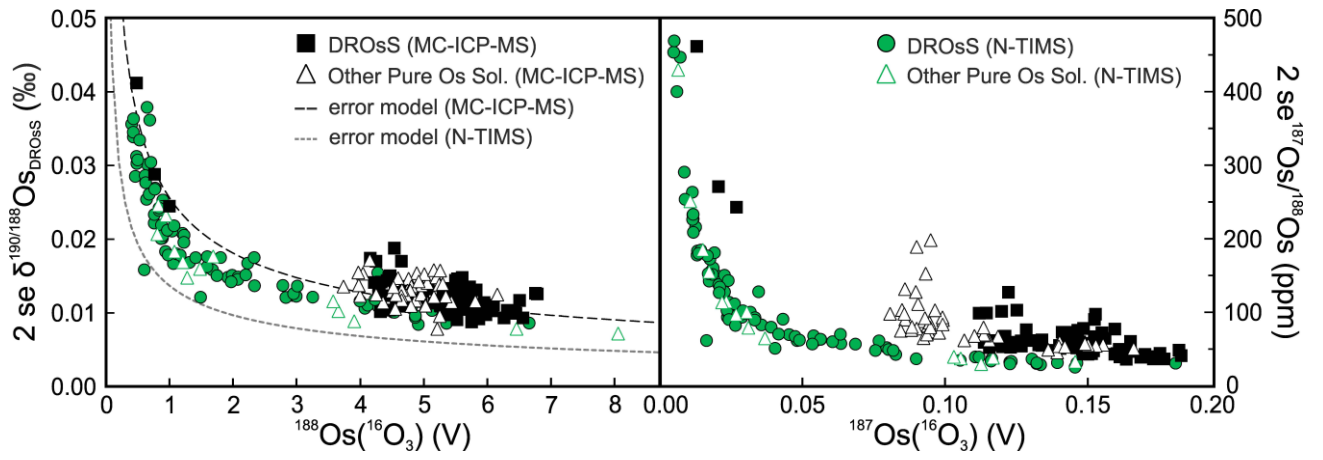
750

Figure 6

753   **Figure 7**

754

Figure 8

Figure 9

759   **Figure 10**

760

Figure 11

763   **Figure 12**

764

$\delta^{190/188}\text{Os}_{\text{DROsS}}$ (‰)
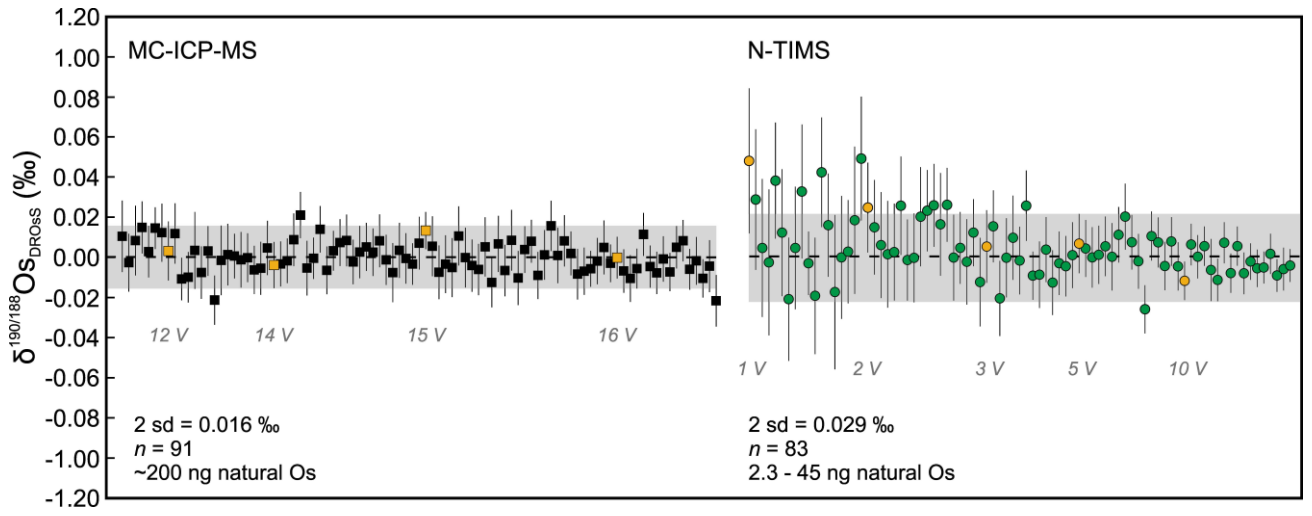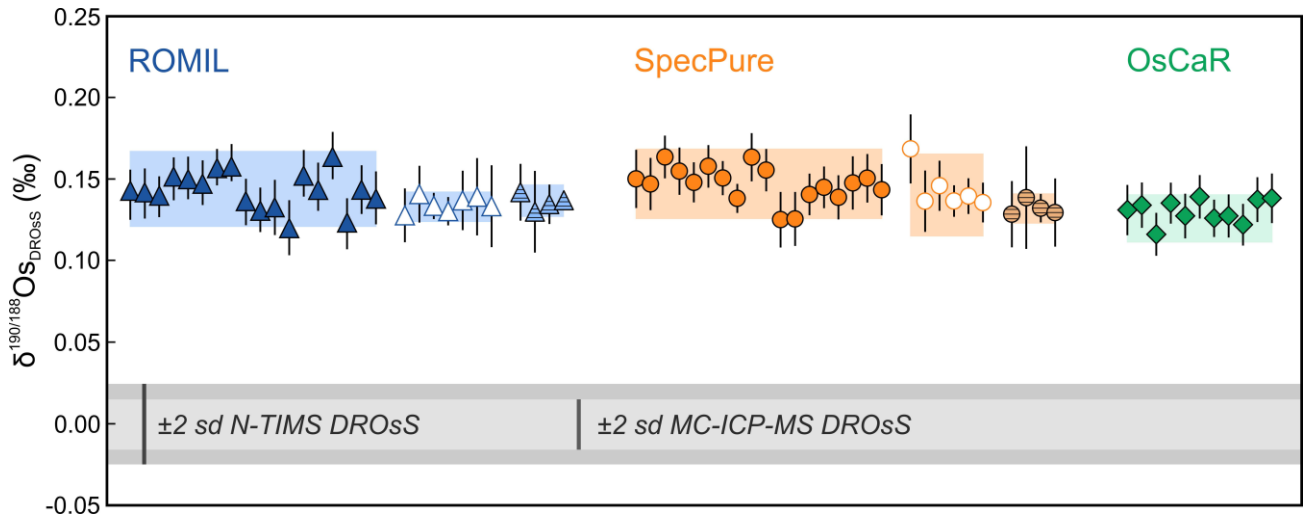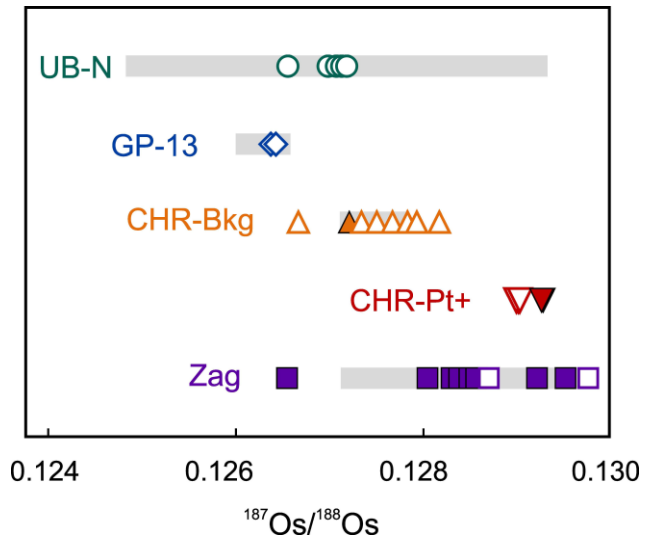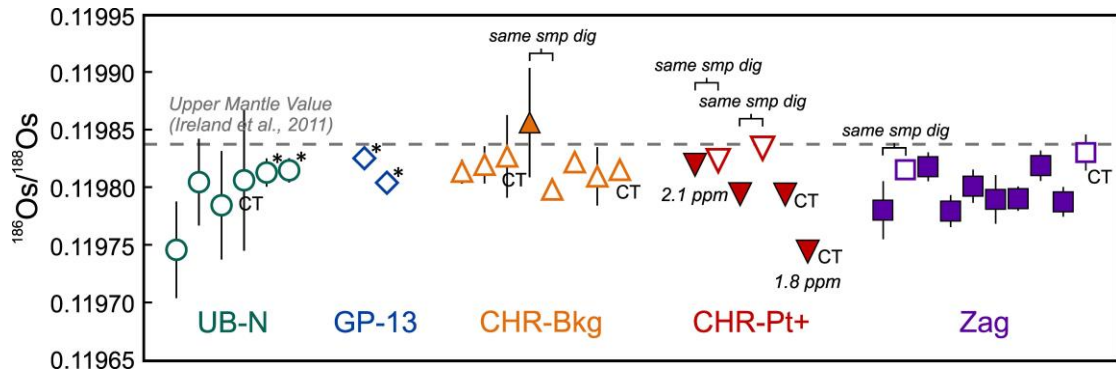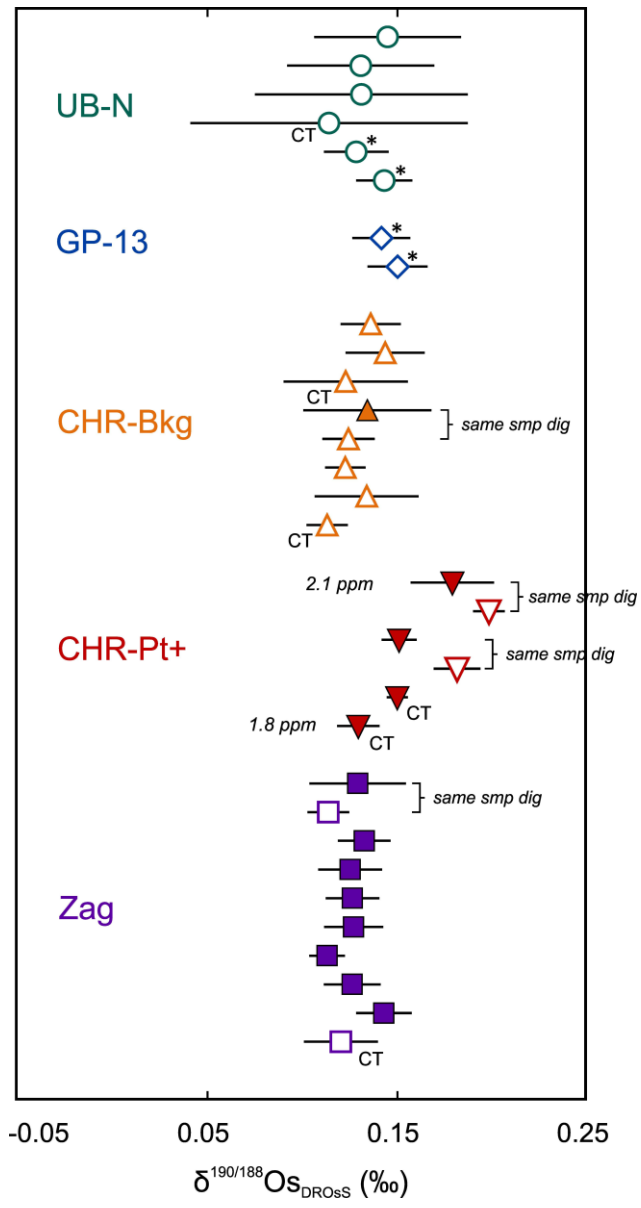
Figure 13
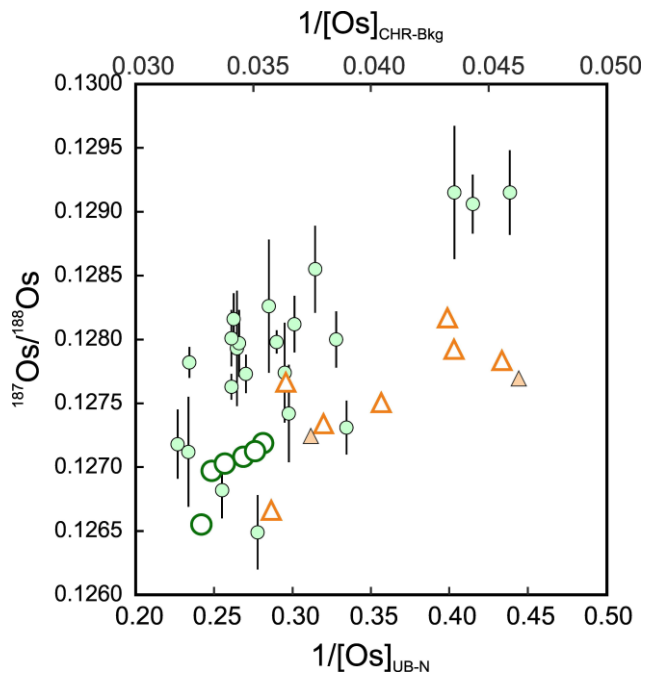
768 **TABLES**

769 **Table 1**

	$^{186}Os/^{188}Os$	$^{187}Os/^{188}Os$	$^{189}Os/^{188}Os$	$^{190}Os/^{188}Os$	$^{192}Os/^{188}Os$
Reference std DROsS (±2 sd)	0.119909 ± 04	0.160916 ± 04	1.219780	1.983979 ± 30	3.083580 ± 14
^{188}Os - ^{190}Os spike (±2 se)	0.001372 ± 54	0.001239 ± 58	0.020944 ± 11	0.684512 ± 06	0.036517 ± 14

770

Table 2

Cup	L4	L3	L2	L1	Ax	H1	H2	H3	H4
MC-ICP-MS									
Analyte isotopes	^{183}W	^{185}Re	^{186}Os	^{187}Os	^{188}Os	^{189}Os	^{190}Os	^{192}Os	^{194}Pt
N-TIMS									
Mass		*232*	*234*	*235*	*236*	*237*	*238*	*240*	
Seq1		^{184}Os^{16}O$_3^-$	^{186}Os^{16}O$_3^-$	^{187}Os^{16}O$_3^-$	^{188}Os^{16}O$_3^-$	^{189}Os^{16}O$_3^-$	^{190}Os^{16}O$_3^-$	^{192}Os^{16}O$_3^-$	
Mass		*236*	*238*	*239*	*240*	*241*	*242*		
Seq2		^{188}Os^{16}O$_3^-$	^{190}Os^{16}O$_3^-$		^{192}Os^{16}O$_3^-$	^{192}Os^{16}O$_2$^{17}O$^-$	^{192}Os^{16}O$_2$^{18}O$^-$		

773 **Table 3**

(i) Signal intensity			
Concentration	**δ^{190}Os**	**2 se**	**^{Total}Os (V)**
0.10 ppm	0.007	0.012	2.71
0.08 ppm	-0.007	0.014	2.08
0.05 ppm	-0.004	0.021	1.31
0.04ppm	-0.014	0.026	1.02
0.03 ppm	0.017	0.033	0.66
0.02 ppm	-0.009	0.045	0.47
0.01 ppm	-0.018	0.055	0.26
0.005 ppm	0.014	0.102	0.14
(ii) Matrix effects and interference corrections			
Doping element	**δ^{190}Os**	**2 se**	
Lith* 5%	-0.009	0.018	
PGE** 5%	-0.008	0.014	
Fe, Ni 5%	-0.001	0.017	
Pt 0.01%	0.005	0.017	
Pt 0.1%	0.012	0.018	
Pt 1%	0.011	0.016	
Pt 10%	-0.001	0.017	
W 0.01%	0.016	0.017	
W 0.1%	0.003	0.015	
W 1%	0.005	0.017	
W 10%	0.020	0.016	
Re 0.01%	0.006	0.012	
Re 0.1%	0.001	0.013	
Re 1%	0.025	0.014	
Re 10%	0.003	0.017	

774

775 **Table 4**

	n	$\delta^{190}Os$	2 sd	$^{187}Os/^{188}Os$	2 sd	$^{186}Os/^{188}Os$	2 sd
DROsS							
DS MC-ICP-MS	91	0.000	0.016	0.160916	0.000020	0.119909	0.000017
DS N-TIMS	83	0.001	0.029	0.160916	0.000043	0.119909	0.000043
un-spiked	14	-	-	0.160919	0.000031	-	-
previous study (MC-ICP-MS; Nowell et al., 2008[35])	21	-	-	0.160924	0.000003	0.119920	0.000002
previous study (N-TIMS; Luguet et al. ,2008[36])	8	-	-	0.160924	0.000004	0.119932	0.000006
ROMIL							
DS MC-ICP-MS	18	0.144	0.023	0.106827	0.000047	0.119806	0.000017
DS N-TIMS	7	0.133	0.009	0.106857	0.000042	0.119803	0.000023
sample-std bracketing MC-ICP-MS	4*	0.137	0.010	0.106861	0.000024	0.119806	0.000007
un-spiked	3	-	-	0.106878	0.000032	-	-
SpecPure							
DS MC-ICP-MS	18	0.147	0.022	0.149162	0.000026	0.119890	0.000019
DS N-TIMS	6	0.140	0.025	0.149161	0.000053	0.119889	0.000031
sample-std bracketing MC-ICP-MS	4*	0.132	0.009	0.149163	0.000012	0.119885	0.000016
un-spiked	3	-	-	0.149180	0.000088	-	-
OsCaR							
DS MC-ICP-MS	11	0.126	0.015	0.128298	0.000022	0.119816	0.000014

776

Table 5

				smp weight (g)	^{total}Os (V)	^{188}Os(O$_3^-$)	^{187}Os (O$_3^-$)	δ^{190}Os	2 se	^{187}Os/^{188}Os	2 se	^{186}Os/^{188}Os	2 se	[Os] ng g^{-1}	2 se
UB-N	1	HPA	N-TIMS	2.51	0.98	0.37	0.008	0.145	0.039	0.126555	0.000040	0.119746	0.000042	4.13	0.002
	2	HPA	N-TIMS	2.51	1.16	0.43	0.009	0.131	0.039	0.126983	0.000039	0.119804	0.000037	4.02	0.002
	3	HPA	N-TIMS	2.49	0.92	0.35	0.007	0.131	0.056	0.127061	0.000047	0.119784	0.000047	3.89	0.003
	4	CT	N-TIMS	2.49	0.82	0.33	0.006	0.114	0.073	0.127073	0.000057	0.119806	0.000061	3.72	0.002
	5*	HPA	N-TIMS	6.03	3.99	1.53	0.030	0.128	0.017	0.127128	0.000011	0.119813	0.000012	3.62	0.001
	6*	HPA	N-TIMS	5.99	3.09	1.19	0.023	0.143	0.015	0.127181	0.000011	0.119815	0.000010	3.55	0.001
w. mean								**0.136**		**0.127126**		**0.119813**		**3.64**	
2 sd								**0.022**		**0.000453**		**0.000053**		**0.46**	
GP-13	1*	HPA	N-TIMS	4.02	4.95	1.87	0.039	0.142	0.015	0.126372	0.000010	0.119825	0.000010	3.87	0.002
	2*	HPA	N-TIMS	4.05	4.67	1.76	0.036	0.150	0.016	0.126426	0.000009	0.119804	0.000009	3.82	0.002
w. mean								**0.146**		**0.126401**		**0.119813**		**3.84**	
2 sd								**0.012**		**0.000077**		**0.000030**		**0.07**	
CHR-Bkg	1	HPA	N-TIMS	0.93	4.68	1.75	0.037	0.136	0.016	0.126667	0.000010	0.119813	0.000010	27.96	0.01
	2	HPA	N-TIMS	0.92	2.74	1.03	0.022	0.144	0.021	0.127671	0.000016	0.119819	0.000016	27.48	0.01
	3	CT	N-TIMS	0.55	1.21	0.46	0.009	0.123	0.033	0.127340	0.000034	0.119827	0.000035	26.32	0.01
	4a	HPA	MC-ICP-MS	2.06	3.42	1.29	0.026	0.134	0.034	0.127210	0.000040	0.119856	0.000047	24.72	0.001
	4b	HPA	N-TIMS	""	6.02	2.30	0.046	0.124	0.014	0.127503	0.000008	0.119798	0.000009	24.72	0.001
	5	HPA	N-TIMS	0.92	9.64	3.80	0.070	0.123	0.011	0.128170	0.000006	0.119822	0.000006	23.11	0.01
	6	CT	N-TIMS	0.58	1.81	0.71	0.013	0.134	0.027	0.127929	0.000025	0.119809	0.000025	22.97	0.01
	7	HPA	N-TIMS	0.92	9.50	3.79	0.067	0.113	0.011	0.127830	0.000006	0.119815	0.000007	21.95	0.01
w. mean								**0.124**		**0.127803**		**0.119818**		**24.73**	
2 sd								**0.020**		**0.000945**		**0.000034**		**4.39**	
CHR-Pt+	1a	HPA	MC-ICP-MS	0.23	15.54	5.62	0.129	0.179	0.022	0.128992	0.000011	0.119819	0.000009	2121	6
	1b	HPA	N-TIMS	""	15.35	5.59	0.129	0.198	0.008	0.129278	0.000004	0.119823	0.000005	2121	4
	2a	HPA	MC-ICP-MS	0.25	25.05	9.41	0.195	0.151	0.009	0.129012	0.000006	0.119794	0.000004	1805	6
	2b	HPA	N-TIMS	""	6.60	2.49	0.052	0.181	0.012	0.129260	0.000008	0.119833	0.000008	1805	6

	3	CT	MC-ICP-MS	0.25	23.15	8.76	0.178	0.150	0.005	0.129029	0.000004	0.119796	0.000003	1785	4
	4	CT	MC-ICP-MS	0.25	12.02	4.54	0.092	0.129	0.011	0.128993	0.000012	0.119744	0.000009	1747	6
w. mean								**0.162**		**0.129033**		**0.119804**		**1879**	
2 sd								**0.051**		**0.000273**		**0.000064**		**349**	
ZAG	1a	HPA	MC-ICP-MS	0.24	6.73	2.51	0.049	0.129	0.025	0.129518	0.000018	0.119780	0.000025	929	6
	1b	HPA	N-TIMS	""	3.28	1.26	0.025	0.114	0.011	0.129759	0.000007	0.119815	0.000007	929	4
	2	HPA	MC-ICP-MS	0.25	8.94	3.28	0.067	0.133	0.014	0.126549	0.000011	0.119818	0.000012	926	6
	3	HPA	MC-ICP-MS	0.25	9.16	3.38	0.068	0.125	0.017	0.128046	0.000014	0.119779	0.000013	905	6
	4	HPA	MC-ICP-MS	0.25	8.63	3.18	0.064	0.126	0.014	0.128557	0.000012	0.119801	0.000014	904	6
	5	HPA	MC-ICP-MS	0.50	5.78	2.15	0.042	0.127	0.016	0.129214	0.000028	0.119789	0.000021	892	3
	6	HPA	MC-ICP-MS	0.50	12.05	4.47	0.088	0.113	0.009	0.128650	0.000011	0.119790	0.000010	887	3
	7	HPA	MC-ICP-MS	0.25	8.73	3.24	0.064	0.126	0.015	0.128382	0.000013	0.119819	0.000013	884	6
	8	HPA	MC-ICP-MS	0.25	9.03	3.40	0.065	0.143	0.015	0.128303	0.000014	0.119787	0.000013	861	6
	9	CT	N-TIMS	0.08	5.05	1.90	0.040	0.120	0.019	0.128699	0.000015	0.119830	0.000015	839	17
w. mean								**0.123**		**0.128407**		**0.119804**		**896**	
2 sd								**0.018**		**0.001791**		**0.000036**		**59**	

778

REFERENCES

1. S. B. Shirey and R. J. Walker, *Annual Review of Earth and Planetary Sciences*, 1998, **26**, 423-500.
2. R. W. Carlson, *Lithos*, 2005, **82**, 249-272.
3. R. J. Walker, M. F. Horan, J. W. Morgan, H. Becker, J. N. Grossman and A. E. Rubin, *Geochimica et Cosmochimica Acta*, 2002, **66**, 4187-4201.
4. T. Meisel, R. J. Walker and J. W. Morgan, *Nature*, 1996, **383**, 517-520.
5. A. D. Brandon, R. J. Walker, J. W. Morgan, M. D. Norman and H. M. Prichard, *Science*, 1998, **280**, 1570-1573.
6. R. J. Walker, *Chemie der Erde-Geochemistry*, 2009, **69**, 101-125.
7. J. E. Snow and L. Reisberg, *Earth and Planetary Science Letters*, 1995, **133**, 411-421.
8. A. Meibom, N. H. Sleep, C. P. Chamberlain, R. G. Coleman, R. Frei, M. T. Hren and J. L. Wooden, *Nature*, 2002, **419**, 705-708.
9. A. D. Brandon, R. A. Creaser, S. B. Shirey and R. W. Carlson, *Science*, 1996, **272**, 861-863.
10. D. G. Pearson, S. W. Parman and G. M. Nowell, *Nature*, 2007, **449**, 202-205.
11. C. W. Dale, A. Gannoun, K. W. Burton, T. W. Argles and I. J. Parkinson, *Earth and Planetary Science Letters*, 2007, **253**, 211-225.
12. H. J. Stein, K. Sundblad, R. J. Markey, J. W. Morgan and G. Motuza, *Mineralium Deposita*, 1998, **33**, 329-345.
13. K. W. Burton, *Journal of Geochemical Exploration*, 2006, **88**, 262-265.
14. W. J. Pegram, S. Krishnaswami, G. E. Ravizza and K. K. Turekian, *Earth and Planetary Science Letters*, 1992, **113**, 569-576.
15. B. Peucker-Ehrenbrink and G. Ravizza, *Terra Nova*, 2000, **12**, 205-219.
16. S. G. Nielsen, M. Rehkämper and A. N. Halliday, *Geochimica et Cosmochimica Acta*, 2006, **70**, 2643-2657.
17. G. A. Brennecka, L. E. Borg, I. D. Hutcheon, M. A. Sharp and A. D. Anbar, *Earth and Planetary Science Letters*, 2010, **291**, 228-233.
18. J. B. Creech, J. A. Baker, M. R. Handler, M. Schiller and M. Bizzarro, *Journal of Analytical Atomic Spectrometry*, 2013, **28**, 853-865.
19. J. B. Creech, J. A. Baker, M. R. Handler and M. Bizzarro, *Chemical Geology*, 2014, **363**, 293-300.
20. C. H. Stirling, M. B. Andersen, E.-K. Potter and A. N. Halliday, *Earth and Planetary Science Letters*, 2007, **264**, 208-225.
21. M. Rehkämper, M. Frank, J. R. Hein, D. Porcelli, A. Halliday, J. Ingri and V. Liebetrau, *Earth and Planetary Science Letters*, 2002, **197**, 65-81.
22. S. G. Nielsen, M. Rehkamper, M. D. Norman, A. N. Halliday and D. Harrison, *Nature*, 2006, **439**, 314-317.
23. J. J. Shen, D. A. Papanastassiou and G. J. Wasserburg, *Geochimica et Cosmochimica Acta*, 1996, **60**, 2887-2900.
24. J. L. Birck, M. R. Barman and F. Capmas, *Geostandards Newsletter*, 1997, **21**, 19-27.
25. M. H. Dodson, *Journal of Scientific Instruments*, 1963, **40**, 289-295.
26. S. J. G. Galer, *Chemical Geology*, 1999, **157**, 255-274.
27. M.-A. Millet, J. A. Baker and C. E. Payne, *Chemical Geology*, 2012, **304**, 18-25.
28. A. D. Brandon, M. Humayun, I. S. Puchtel, I. Leya and M. Zolensky, *Science*, 2005, **309**, 1233-1236.
29. T. Yokoyama, V. K. Rai, C. M. D. Alexander, R. S. Lewis, R. W. Carlson, S. B. Shirey, M. H. Thiemens and R. J. Walker, *Earth and Planetary Science Letters*, 2007, **259**, 567-580.
30. T. Yokoyama, C. M. D. Alexander and R. J. Walker, *Earth and Planetary Science Letters*, 2010, **291**, 48-59.
31. N. Wittig, M. Humayun, A. D. Brandon, S. Huang and I. Leya, *Earth and Planetary Science Letters*, 2013, **361**, 152-161.
32. C. Siebert, T. F. Nägler and J. D. Kramers, *Geochemistry, Geophysics, Geosystems*, 2001, **2**, 1032.
33. M.-A. Millet and N. Dauphas, *Journal of Analytical Atomic Spectrometry*, 2014, **29**, 1444-1458.
34. M.-A. Millet, N. Dauphas, N. D. Greber, K. W. Burton, C. W. Dale, B. Debret, C. G. Macpherson, G. M. Nowell and H. M. Williams, *Earth and Planetary Science Letters*, 2016, **449**, 197-205.
35. J. F. Rudge, B. C. Reynolds and B. Bourdon, *Chemical Geology*, 2009, **265**, 420-431.

835   36.   G. M. Nowell, A. Luguet, D. G. Pearson and M. A. Horstwood, *Chemical Geology*, 2008, **248**,
836   363-393.
837   37.   A. Luguet, G. M. Nowell and D. G. Pearson, *Chemical Geology*, 2008, **248**, 342-362.
838   38.   J. Liu and D. G. Pearson, *Chemical Geology*, 2014, **363**, 301-311.
839   39.   R. Chatterjee and J. C. Lassiter, *Chemical Geology*, 2015, **396**, 112-123.
840   40.   T. Meisel, L. Reisberg, J. Moser, J. Carignan, F. Melcher and G. Brügmann, *Chemical geology*,
841   2003, **201**, 161-179.
842   41.   D. G. Pearson, G. J. Irvine, D. A. Ionov, F. R. Boyd and G. E. Dreibus, *Chemical Geology*, 2004,
843   **208**, 29-59.
844   42.   P. J. Potts, C. J. B. Gowing and K. Govindaraju, *Geostandards Newsletter*, 1992, **16**, 81-108.
845   43.   V. Paliulionyte, T. Meisel, P. Ramminger and P. Kettisch, *Geostandards and Geoanalytical*
846   *Research*, 2006, **30**, 87-96.
847   44.   T. Meisel, J. Moser, N. Fellner, W. Wegscheider and R. Schoenberg, *Analyst*, 2001, **126**, 322-
848   328.
849   45.   S. B. Shirey and R. J. Walker, *Analytical Chemistry*, 1995, **67**, 2136-2141.
850   46.   A. S. Cohen and F. G. Waters, *Analytica Chimica Acta*, 1996, **332**, 269-275.
851   47.   M. Roy-Barman, Thesis, Université de Paris VII, 1993.
852   48.   C. W. Dale, K. W. Burton, D. G. Pearson, A. Gannoun, O. Alard, T. W. Argles and I. J. Parkinson,
853   *Geochimica et Cosmochimica Acta*, 2009, **73**, 1394-1416.
854   49.   R. A. Creaser, D. A. Papanastassiou and G. J. Wasserburg, *Geochimica et Cosmochimica Acta*,
855   1991, **55**, 397-401.
856   50.   F. Albarède and B. Beard, *Reviews in Mineralogy and Geochemistry*, 2004, **55**, 113-152.
857   51.   Y. Nagai and T. Yokoyama, *Journal of Analytical Atomic Spectrometry*, 2016, **31**, 948-960.
858   52.   E. A. Worsham, R. J. Walker and K. R. Bermingham, *International Journal of Mass Spectrometry*,
859   2016, **407**, 51-61.
860   53.   Y. Liu, M. Huang, A. Masuda and M. Inoue, *International Journal of Mass Spectrometry and Ion*
861   *Processes*, 1998, **173**, 163-175.
862   54.   Z.-Y. Chu, C.-F. Li, Z. Chen, J.-J. Xu, Y.-K. Di and J.-H. Guo, *Analytical chemistry*, 2015.
863   55.   K. R. Bermingham, R. J. Walker and E. A. Worsham, *International Journal of Mass Spectrometry*,
864   2016, **403**, 15-26.
865   56.   A. Trinquier, M. Touboul and R. J. Walker, *Analytical chemistry*, 2016, **88**, 1542-1546.
866   57.   R. N. Clayton, L. Grossman and T. K. Mayeda, *Science*, 1973, **182**, 485-488.
867   58.   E. Barkan and B. Luz, *Rapid Communications in Mass Spectrometry*, 2005, **19**, 3737-3742.
868   59.   D. Rumble, M. F. Miller, I. A. Franchi and R. C. Greenwood, *Geochimica et Cosmochimica Acta*,
869   2007, **71**, 3592-3600.
870   60.   I. Ahn, J. I. Lee, M. Kusakabe and B.-G. Choi, *Geosciences Journal*, 2012, **16**, 7-16.
871   61.   R. J. Walker, A. D. Brandon, J. M. Bird, P. M. Piccoli, W. F. McDonough and R. D. Ash, *Earth and*
872   *Planetary Science Letters*, 2005, **230**, 211-226.
873   62.   D. G. Pearson and S. J. Woodland, *Chemical Geology*, 2000, **165**, 87-107.
874   63.   L. P. Bédard and S.-J. Barnes, *Geostandards and Geoanalytical Research*, 2004, **28**, 311-316.
875   64.   T. J. Ireland, R. J. Walker and A. D. Brandon, *Geochimica et Cosmochimica Acta*, 2011, **75**, 4456-
876   4475.
877   65.   L. Reisberg and T. Meisel, *Geostandards Newsletter*, 2002, **26**, 249-267.
878   66.   A. Ishikawa, R. Senda, K. Suzuki, C. W. Dale and T. Meisel, *Chemical Geology*, 2014, **384**, 27-46.
879   67.   R. A. Lord, H. M. Prichard and C. R. Neary, *Transactions - Institution of Mining & Metallurgy,*
880   *Section B*, 1994.
881   68.   M. Griselin, J. Van Belle, C. Pomies, P. Vroon, M. Van Soest and G. Davies, *Chemical Geology*,
882   2001, **172**, 347-359.
883   69.   V. Chavagnac, Université Rennes 1, 1998.
884   70.   M. Thirlwall, *Chemical Geology*, 1991, **94**, 13-22.
885   71.   L. Reisberg and A. Zindler, *Earth and Planetary Science Letters*, 1986, **81**, 29-45.
886   72.   G. Wasserburg, S. Jacobsen, D. DePaolo, M. McCulloch and T. Wen, *Geochimica et*
887   *Cosmochimica Acta*, 1981, **45**, 2311-2323.
888   73.   A. O. Nier, *Physical Review*, 1950, **77**, 789.
889   74.   J. Harvey, C. W. Dale, A. Gannoun and K. W. Burton, *Geochimica et Cosmochimica Acta*, 2011,
890   **75**, 5574-5596.
891   75.   I. S. Puchtel, M. Humayun and R. J. Walker, *Precambrian Research*, 2007, **158**, 119-137.

892 76. C. Marchesi, C. W. Dale, C. J. Garrido, D. G. Pearson, D. Bosch, J.-L. Bodinier, F. Gervilla and K.
893 Hidas, *Earth and Planetary Science Letters*, 2014, **400**, 33-44.
894
895
896

897 **Electronic Supplementary Information**

898 **S.1. Oxygen corrections for N-TIMS analyses**

899 An important step in the N-TIMS data reduction, is the correction for oxygen interferences. In this study,

900 we have applied a two-step correction, where in step one a starting oxygen composition is used in order

901 to determine the "true" oxygen isotope composition of the particular measurement. For the first step

902 we have used the compositions as determined by Luguet et al. (2008):

903 $\qquad$ $^{17}O/^{16}O_{Luguet} = R_1 = 0.00038582$ $\qquad$ (1)

904 $\qquad$ $^{18}O/^{16}O_{Luguet} = R_2 = 0.00203486$ $\qquad$ (2)

905 The intensities obtained on a certain mass (I_x in V) were corrected for the effects of variable isobaric

906 oxygen isotope interferences of the heavier oxygen isotopes (^{17}O and ^{18}O) following:

907 $\qquad$ $O_1 = 3*R_1$ $\qquad$ (3)

908 $\qquad$ $O_2 = 3*R_1^2 + 3*R_2$ $\qquad$ (4)

909 $\qquad$ $O_3 = R_1^3 + 6*R_1*R_2$ $\qquad$ (5)

910 $\qquad$ $O_4 = 3*R_1^2*R_2 + 3*R_2^2$ $\qquad$ (6)

911 $\qquad$ $O_5 = 3*R_1*R_2^2$ $\qquad$ (7)

912 $\qquad$ $O_6 = R_2^3$ $\qquad$ (8)

913 $\qquad$ Where O_i represent the difference in mass (i in amu) between the analyte mass of interest and

914 the lightest mass that could generate a potential oxide interference. For example, the ions collected on

915 mass 234 (I_{234}) are predominantly representing $^{186}Os^{16}O_3^-$ (I^{186}) ions but also reflect oxygen complexes

916 originating from ^{184}Os ($^{184}Os^{16}O^{17}O_2^-$ and $^{184}Os^{16}O_2^{18}O^-$). In this case, the mass difference is 2 amu and

917 thus $O_i = O_2$. Using equations 3-8, the intensities of $^{j}Os^{16}O_3^-$ ions (I^j) can be determined as follows:

918 $\qquad$ $I^{184} = I_{232}$ $\qquad$ (9)

919 $\qquad$ $I^{186} = I_{234} - (I_{232}*O_2)$ $\qquad$ (10)

920 $\qquad$ $I^{187} = I_{235} - (I_{232}*O_3) - (I_{234}*O_1)$ $\qquad$ (11)

921 $\qquad$ $I^{188} = I_{236} - (I_{232}*O_4) - (I_{234}*O_2) - (I_{235}*O_1)$ $\qquad$ (12)

922 $\qquad$ $I^{189} = I_{237} - (I_{232}*O_5) - (I_{234}*O_3) - (I_{235}*O_2) - (I_{236}*O_1)$ $\qquad$ (13)

923 $\qquad$ $I^{190} = I_{238} - (I_{232}*O_6) - (I_{234}*O_4) - (I_{235}*O_3) - (I_{236}*O_2) - (I_{237}*O_1)$ $\qquad$ (14)

924 $\qquad$ $I^{192} = I_{240} - (I_{234}*O_6) - (I_{235}*O_5) - (I_{236}*O_4) - (I_{237}*O_3) - (I_{238}*O_2)$ $\qquad$ (15)

925 By obtaining the intensities on the various $^{j}Os^{16}O_3^-$ ions, masses 241 ($^{192}Os^{16}O_2^{17}O^- = I^{192}17$) and 242

926 ($^{192}Os^{16}O_2^{18}O^- = I^{192}18$) can be stripped from minor tri-oxide interferences as well, following:

927 $\qquad$ $I^{192}17 = I_{241} - (I_{235}*O_6) - (I_{236}*O_5) - (I_{237}*O_4) - (I_{238}*O_3)$ $\qquad$ (16)

928 $\qquad$ $I^{192}18 = I_{242} - (I_{236}*O_6) - (I_{237}*O_5) - (I_{238}*O_4)$ $\qquad$ (17)

929 Subsequently, these intensities were used to determine the "true" oxygen isotope compositions

930 ($^{17}O/^{16}O$ and $^{18}O/^{16}O$) of the individual cycle:

931          $^{17}O/^{16}O_{true} = R'_1 = (I^{192}17 \, / \, I^{192}) \, / \, 3$ (18)

932          $^{18}O/^{16}O_{true} = R'_2 = (I^{192}18 \, / \, I^{192}) \, / \, 3$ (19)

933 These oxygen compositions were then used to perform the "stripping" again (equations 3-15), now with

934 the "true" oxygen composition. This means that R_1 and R_2 in equations 3-8 are replaced by R'_1 and R'_2.

935   In this study, we observed that the $^{17}O/^{16}O$ composition imposes a significant inaccuracy on the

936 stable Os isotope composition when total Os signal intensities dropped below 1 V. Therefore, instead

937 of accomplishing equations (16) and (18), the $^{17}O/^{16}O$ composition was based on the "true or measured"

938 $^{18}O/^{16}O$ composition as determined in equation (19). In order to calculate the $^{17}O/^{16}O$ from the

939 measured $^{18}O/^{16}O$ the relationship between the stable oxygen isotopes needs to be considered. In this

940 study, we assume that the oxygen isotopic compositions vary as a result of equilibrium mass-dependent

941 isotopic fractionation. The relationship among the three stable oxygen isotopes is exponential and can

942 be written as:

943          $\delta^{17}O + 1 = \left(\delta^{18}O + 1\right)^{\lambda}$ (20)

944 , where λ defines the slope of the line. By taking a logarithm, equation (20) can be linearized (Miller,

945 2002[1]):

946          $10^3 * ln\left(\delta^{17}O/10^3 + 1\right) = \lambda * \left(10^3 * ln\left(\delta^{18}O/10^3 + 1\right)\right)$ (21)

947 To calculate the $^{17}O/^{16}O$ composition, equation (21) can be re-written:

948          $\delta^{17}O = e^{\lambda*\left(ln\left(\left(\delta^{18}O/10^3\right)+1\right)\right)} * 10^3$ (22)

949 with,

950          $^{17}O/^{16}O_{true} = \left(\delta^{17}O/10^3 + 1\right) * \, ^{17}O/^{16}O_{VSMOW}$ (23)

951 , where λ is 0.526, as we assume that the fractionation occurs along the "Terrestrial Fractionation Line"

952 (TFL[2]) for which the average literature values is 0.526 [e.g. 3-5]. The $\delta^{17}O$ and $\delta^{18}O$ use the VSMOW (Vienna

953 Standard Mean Ocean Water) as reference values. Generally, the $^{18}O/^{16}O$ ratio of VSMOW is accepted

954 to be 0.0020052[6] whereas there is more debate about the $^{17}O/^{16}O$ ratio, with values ranging between

955 0.000380[7] and 0.000384[8]. Using data of this study we obtain an intercept with zero at a value of

956 0.000382 which is within the range previously observed and, therefore, used in this study (Fig. S.1). To

957 determine this intercept we used analyses that were obtained at a beam intensity of >2 mV on mass

958 241. If these analyses are plotted in $10^3 \, ln(1+\delta^{17}O/10^3)$ vs. $10^3 \, ln(1+ \delta^{18}O/10^3)$ space, following the

959 approach of Miller (2002)[1], a regression coefficient (λ) of 0.488±0.072 (95 c.i.) is obtained (Fig. S.1).

960 Isoplot 4 was used to calculate the slope as well as the error on the slope. When the selected analyses

961 are considered in $^{17}O/^{16}O$ vs. $^{18}O/^{16}O$ space an approximate linear relationship with a slope of 0.092 ±

962 0.014 (95 c.i.) and an intercept of 0.000197 ± 0.000027 (95 c.i.) is obtained. This is within error of the

963 values obtained when assuming a slope of 0.526 over the $^{18}O/^{16}O$ interval of 0.002007 to 0.002055 (the

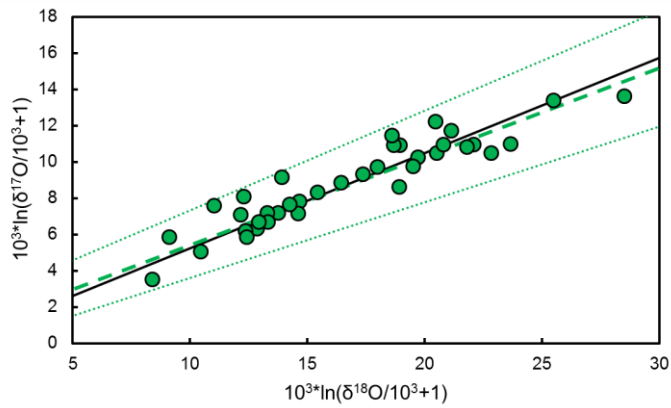964 range in $^{18}O/^{16}O$ observed in this study); 0.0994 x + 0.000183, where x is $^{18}O/^{16}O$.

965

Figure S.1 Measured $^{17}O/^{16}O$ and $^{18}O/^{16}O$ compositions of analyses with a beam intensity of >2 mV on mass 241 plotted as delta values in logarithmic form. The regression line (dashed line) is within error (dotted lines) of the terrestrial fractionation line with a slope of 0.526 (solid line).

975

976 **REFERENCES**
977 1. M. F. Miller, *Geochimica et Cosmochimica Acta*, 2002, **66**, 1881-1889.
978 2. R. N. Clayton, L. Grossman and T. K. Mayeda, *Science*, 1973, **182**, 485-488.
979 3. E. Barkan and B. Luz, *Rapid Communications in Mass Spectrometry*, 2005, **19**, 3737-3742.
980 4. D. Rumble, M. F. Miller, I. A. Franchi and R. C. Greenwood, *Geochimica et Cosmochimica Acta*,
981 2007, **71**, 3592-3600.
982 5. I. Ahn, J. I. Lee, M. Kusakabe and B.-G. Choi, *Geosciences Journal*, 2012, **16**, 7-16.
983 6. P. Baertschi, *Earth and Planetary Science Letters*, 1976, **31**, 341-344.
984 7. W. J. Li, B. L. Ni, D. Q. Jin and Q. G. Zhang, *Kexue Tongbao*, 1988, **33**, 1610-1613.
985 8. J. C. Lorin, *Chemical Geology: Isotope Geoscience section*, 1992, **101**, 193-195.

986

987